UNIVERSITY of York

This is a repository copy of *POP-type ligands:Variable coordination and hemilabile behaviour*.

White Rose Research Online URL for this paper:
https://eprints.whiterose.ac.uk/id/eprint/155087/

Version: Published Version

Article:
Adams, Gemma M. and Weller, Andrew S. orcid.org/0000-0003-1646-8081 (2018) POP-type ligands:Variable coordination and hemilabile behaviour. COORDINATION CHEMISTRY REVIEWS. pp. 150-172. ISSN: 0010-8545

https://doi.org/10.1016/j.ccr.2017.08.004

Reuse
This article is distributed under the terms of the Creative Commons Attribution (CC BY) licence. This licence allows you to distribute, remix, tweak, and build upon the work, even commercially, as long as you credit the authors for the original work. More information and the full terms of the licence here: https://creativecommons.org/licenses/

Takedown
If you consider content in White Rose Research Online to be in breach of UK law, please notify us by emailing eprints@whiterose.ac.uk including the URL of the record and the reason for the withdrawal request.

White Rose university consortium
Universities of Leeds, Sheffield & York

eprints@whiterose.ac.uk
https://eprints.whiterose.ac.uk/

Coordination Chemistry Reviews 355 (2018) 150–172

Contents lists available at ScienceDirect

Coordination Chemistry Reviews

journal homepage: www.elsevier.com/locate/ccr

Review

POP-type ligands: Variable coordination and hemilabile behaviour

Gemma M. Adams *, Andrew S. Weller *

Department of Chemistry, Chemistry Research Laboratory, University of Oxford, Mansfield Road, Oxford OX1 3TA, UK

ARTICLE INFO

Article history:
Received 15 June 2017
Received in revised form 4 August 2017
Accepted 6 August 2017
Available online 1 September 2017

Dedicated to Prof. Pierre Braunstein on the occasion of his 70th birthday.

Keywords:
Hemilabile ligands
Variable coordination modes
Xantphos
DPEphos
POP ligands
Catalysis

ABSTRACT

Hemilabile ligands – ligands containing two or more potential donors to a metal centre, of which one or more can dissociate – have the ability to provide a transition metal complex with open coordination sites at which reactivity can occur, or stabilise low coordinate intermediates along reaction pathways. POP-type ligands and in particular POP, Xantphos, DBFphos and DPEphos-based ligands contain three possible binding sites: two phosphines and an ether linker, thus have the potential to show κ^1-, κ^2- or κ^3-binding modes. This review summarises the examples where POP-type ligands display hemilabile, or closely related variable coordination, characteristics in either synthesis or catalysis.
© 2017 The Authors. Published by Elsevier B.V. This is an open access article under the CC BY license (http://creativecommons.org/licenses/by/4.0/).

Contents

1. Introduction

The importance of transition-metal complexes in homogeneous catalysis cannot be over-stated. The ability to precisely control at the atomic level the structure of a catalyst through manipulation of both the metal and – perhaps more importantly – the supporting ligands is central to the development and utilisation of such catalysts in a myriad of applications for the synthesis of fine– or commodity–chemicals or new materials. [1]. Bidentate diphosphine-based ligands have played a particularly important role in processes catalysed by later transition metals, such as alkene hydrogenation, hydroformylation, cross-coupling and carbonylations [2]. Fine control of the metal–ligand environment through bite angle effects or the steric profile of phosphine substituents provides the ability to control turnover- and product-determining steps [3,4]. Tridentate pincer-type ligands have also

* Corresponding authors.
E-mail addresses: gemma.adams@chem.ox.ac.uk (G.M. Adams), andrew.weller@chem.ox.ac.uk (A.S. Weller).

http://dx.doi.org/10.1016/j.ccr.2017.08.004
0010-8545/© 2017 The Authors. Published by Elsevier B.V.
This is an open access article under the CC BY license (http://creativecommons.org/licenses/by/4.0/).

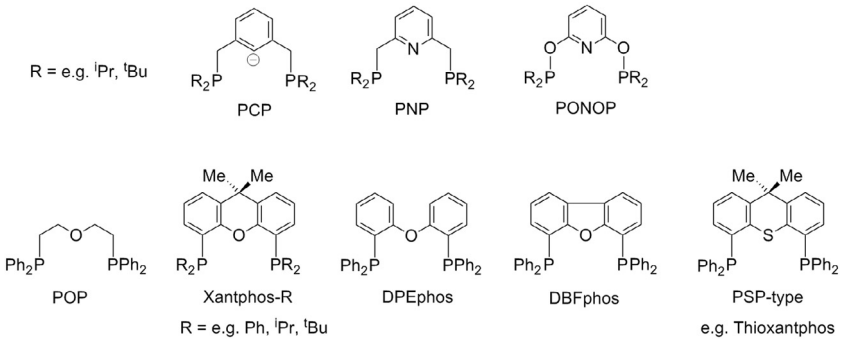

Fig. 1. Pincer-type, POP-type and PSP-type ligands.

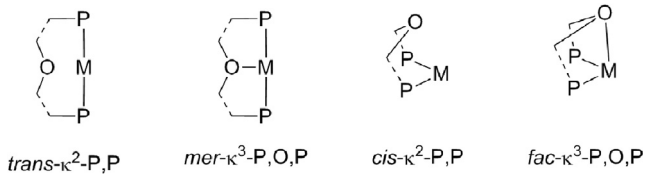

Fig. 2. Ligand flexibility and hemilability in POP-type ligands.

played an increasingly dominant role in catalysis [5,6], owing to their stability, ability to define a particular coordination geometry in which the pincer ligand occupies three *meridional* sites around a metal centre, and in some cases ability to take part in metal–ligand cooperative reactivity [7]. Although, again, there are many examples of the use of pincer-ligand complexes, those based around "PCP", "PNP" or "PONOP" (Fig. 1) have found particular applications in alkane dehydrogenation when partnered with iridium, or in the activation of strong bonds and subsequent catalytic transformations more generally [8–10]. These ligands occupy such a "privileged" volume of chemical space due, in large part, to the robust coordination framework that the PNP or PCP ligand motif provides, although the role that coordination flexibility has in certain pincer-ligand classes is also being recognised as being potentially important [11].

The coordination chemistry of tridentate ligands based upon diphosphine ligand frameworks with an additional ether linkage, the so-called "POP" ligands (Fig. 1), has been known for some decades. Their use in catalysis has been significant, especially ligand frameworks based around Xantphos and DPEphos – originally developed as wide bite angle bidentate ligands for rhodium-catalysed hydroformylation [12]. Although principally bidentate in coordination mode, their ability to coordinate the central ether gives ligand geometries that are related to classical tridentate PCP or PNP pincer ligands. If coordination of any of the three ligating atoms was flexible, this offers the ability of the ligand set to adapt to the specific requirements of the metal (i.e. variable oxidation states and resulting geometric constraints), including the binding/release of co-ligands, substrates or products during synthesis, or more importantly during a catalytic cycle. When such flexibility also involves the reversible decoordination of a donor-group, this leads to hemilabile behaviour, in which a metal centre is rendered operationally unsaturated by the temporary decoordination of a ligand, but one that still remains associated with the coordination sphere of the metal. This flexibility, potentially, leads to a number of coordination modes as outlined in Fig. 2. The term hemilabile was introduced by Jeffrey and Rauchfuss in 1979 to describe coordination modes of *ortho*-substituted diphenylanisole ligands [13]. Since then many examples of hemilabile ligand behaviour have been reviewed, amongst others by Lindner in 1991 [14], Mirkin in 1999 [15], Braunstein in 2001 [16], Bassetti in 2006 [17], Mirkin in 2008 (so-called weak link approach to supramolecular complexes) [18] and Hor in 2007 [19]. Interestingly, the potential for hemilability in POP, Xantphos or DPEphos-type ligands was not generally commented upon, but in the last decade this variability in ligand binding has become increasingly recognised. In this contribution we survey the coordination chemistry of such ligands and outline cases where changes in coordination geometry lead to changes in ligand denticity that are directly related to the potential for these ligands to behave in a hemilabile manner. Although when rigorously defined hemilabile refers to the ability to *reversibly* decoordinate a donor group [16], we also survey examples where decoordination may also be irreversible, but focus in these cases on situations where the POP ligand changes its binding mode to accommodate the reaction course. We also briefly comment upon the coordination modes of PSP-type ligands (Fig. 1), however examples of transition metal complexes using this ligand type are much rarer than their POP-type analogues.

2. POP-type ligands

The first crystallographically characterised example of a POP ligand (POP-R = $[R_2P(CH_2)_2]_2O$) bound to a transition metal centre in a κ^3-P,O,P-tridentate manner, through both phosphine groups and the ether linker, was established by Alcock, Brown and co-workers [20,21]. In this example, *trans*-Rh(Cl)(CO)(κ^2-P,P-POP-Ph) (**1**), in which the POP-Ph ligand behaves as a bidentate ligand, underwent chloride abstraction using Ag[PF_6] to yield the cationic, crystallographically characterised, κ^3-P,O,P-POP-Ph complex, *mer*-[Rh(CO)(κ^3-P,O,P-POP-Ph)][PF_6] (**2**) (Scheme 1). At this time, ether

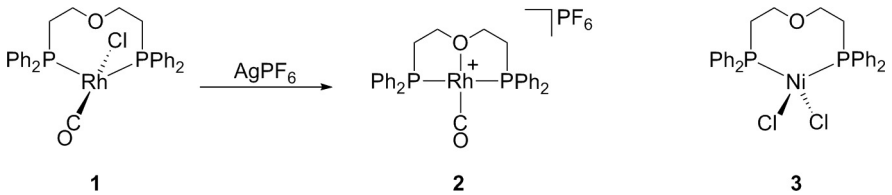

Scheme 1. The reaction of the κ^2-P,P-POP-Ph complex **1** to give the κ^3-P,O,P-POP-Ph complex **2**, and the contrasting structure of **3**.

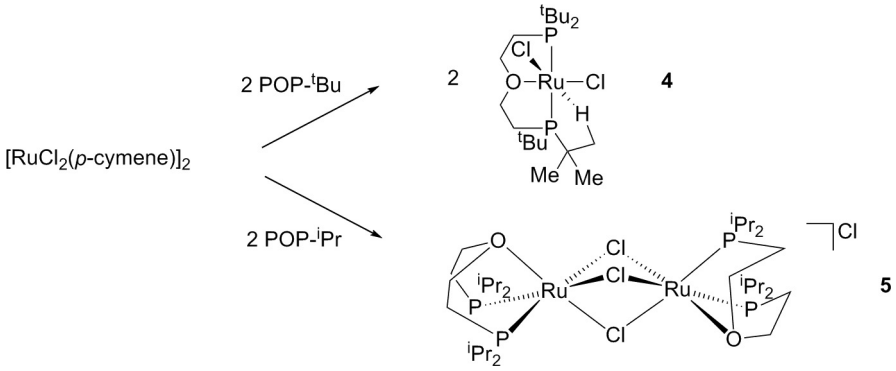

Scheme 2. The difference in reactivity of ruthenium complexes of the POP-^{t}Bu ligand versus its less sterically bulky ^{i}Pr analogue.

complexes of transition metals were relatively rare, and the authors suggested that the chelation effect of the POP-Ph ligand enabled stabilisation of a Rh—O bond in complex **2**. Complex **2** displayed a Rh—O bond distance (2.112(7) Å) and a P—Rh—P bite angle (165.9(1)°) consistent with κ^3-P,O,P-tridentate binding of the ligand. This work contrasted with earlier studies carried out by Greene et al. [22], where structurally characterised *cis*-$NiCl_2$(κ^2-P,P-POP-Ph) (**3**) showed bidentate donation of POP-Ph to a tetrahedral Ni(II) centre (Ni···O = 3.640 Å, P—Ni—P = 107.1(1)°).

Coordination of the ether linker of the POP-R ligand to a transition metal centre was also noted by Gusev [23]. Replacement of the phenyl substituents on the phosphines with alkyl groups led to interesting substituent effects, as demonstrated by the reaction of $[RuCl_2(p\text{-cymene})]_2$ with POP-^{t}Bu versus reaction with POP-^{i}Pr (Scheme 2). The complex derived from POP-^{t}Bu formed a monomeric, formally 16-electron species, *mer*-Ru(Cl)$_2$(κ^3-P,O,P-POP-^{t}Bu) (**4**), which showed approximately octahedral geometry around the Ru centre, stabilised by *mer*-κ^3-P,O,P coordination of POP-^{t}Bu, with the sixth coordination site occupied by a C—H···Ru agostic bond from one of the ^{t}Bu groups of the ligand (Ru—O = 2.123(2) Å, P—Ru—P = 161.1(1)°). In comparison, the equivalent reaction with the less sterically bulky POP-^{i}Pr ligand yielded a bimetallic complex, *fac*-$[Rh_2(\mu\text{-}Cl)_3(\kappa^3\text{-P,O,P-POP-}^{i}Pr)_2][Cl]$ (**5**), which was crystallographically characterised as its $[PF_6]^-$ salt, and showed *fac*-κ^3-P,O,P binding of the POP-^{i}Pr ligand (Ru—O = 2.136(6) Å, P—Ru—P = 101.8(1)°). Whilst both complexes allowed tridentate donation by the ligands, evidenced by the short Ru—O bonds in each case, the wider P—Ru—P bite angle characteristic of *mer*-κ^3-P,O,P coordination of POP-^{t}Bu in complex **4** was favoured over *fac*-κ^3-P,O,P, presumably due to the increased steric bulk of ^{t}Bu compared to ^{i}Pr. The authors postulated that the monomeric κ^3-P,O,P-POP-^{t}Bu complex **4** was formed by dissociation of an initially formed (but not observed) bimetallic POP-^{t}Bu analogue of complex **5**, *fac*-$[Rh_2(\mu\text{-}Cl)_3(\kappa^3\text{-P,O,P-POP-}^{t}Bu)_2][Cl]$. The dissociation of the dinuclear species *via* chloride association to two *mer*-Ru(Cl)$_2$(κ^3-P,O,P-POP-^{t}Bu) monomers was driven by the dimer's inherent instability, caused by the large ^{t}Bu substituents. Further reactivity studies of both complexes **4** and **5** with H_2 and N_2 gave rise to octahedral *mer*-κ^3-P,O,P-coordinated complexes.

Duatti and co-workers have noted the existence of *fac*–*mer* isomerisation in group-7 nitrido complexes M(N)(Cl)$_2$(κ^3-P,O,P-POP-Ph) complexes (M = Tc, Re), Scheme 3 [24,25]. The kinetically favoured *fac*-isomer (**6**) was synthesised at relatively low temperatures, however at elevated temperatures in acetonitrile solvent, the *mer*-isomer (**7**) was irreversibly formed. This was confirmed by NMR spectroscopy, and supported by computational studies of the Tc complexes in which *mer*-Tc(N)(Cl)$_2$(κ^3-P,O,P-POP-Ph) was thermodynamically favoured over the *fac*-isomer by 5.9 kcal mol^{-1}. Whilst neither of the *fac*-isomers of Tc or Re could be characterised by X-ray diffraction studies, hence the presence of a M—O bond in a *fac*-κ^3-P,O,P conformation could not be confirmed, the crystal structures of both *mer*-Tc(N)(Cl)$_2$(κ^3-P,O,P-POP-Ph) [24] and *mer*-Re(N)(Cl)$_2$(κ^3-P,O,P-POP-Ph) [25] were obtained. The P—M—P bond angles of the Tc and Re complexes were 152.1(1)° and 152.7(1)° respectively, with the phosphine ligands *trans* to one another. However, the M—O bond distances were considerably longer than expected: 2.500(4) Å for the Tc complex and 2.505(9) Å for Re. This was proposed to be due to the strong *trans*-labilising effect exerted by the nitrido group, resulting in, an at best weak, M—O interaction. The *fac*–*mer* isomerisation process was proposed to involve dissociation of the ether linker and rearrangement of the resulting square pyramidal structure. Further reactivity of both isomers showed that the *fac*-isomer can undergo a ligand substitution reaction with *S*-methyl 2-methyldithiocarbazate and $Na[BF_4]$ to form complex **8** (Scheme 3) in refluxing CH_2Cl_2/ethanol, whereas *mer*-M(N)(Cl)$_2$(κ^3-P,O,P-POP-Ph), **7**, was found to be unreactive under the same conditions. This difference in reactivity was suggested to be due to a very low lying LUMO, coupled with steric constraints, for the *mer*-isomer.

van Leeuwen et al. utilised the POP-Ph ligand (and derivatives thereof) complexed with rhodium in hydroformylation catalysis [26]. Interestingly, whilst the activity of these complexes were comparable to those of the well-studied Xantphos-Ph ligand (though their selectivity for linear versus branched aldehyde products was moderate in comparison), very little isomerisation (≤0.8%) of the starting 1-alkene was observed when using POP-Ph instead of Xantphos-Ph. The authors speculated that this occurred because the POP-Ph ligand could act in a hemilabile manner [13], and utilise its ability to bind strongly in both bidentate and tridentate fashions in order to occupy any vacant sites formed during the catalytic cycle. The binding of the ether linker of POP-Ph was suggested to be capable of suppressing any *beta*-hydride-elimination events which would form unwanted internal alkenes (Scheme 4).

The study of potential for hemilability in POP-Ph was investigated by Weller and co-workers during their studies of the hydroacylation reaction, which involves the formal addition of a C—H bond across an alkene or alkyne [27]. Previous work had demonstrated that a hemilabile DPEphos ligand (see Schemes 28 and 29) enabled the stabilisation of important intermediates during catalysis, as well as suppressing unwanted reductive decarbonylation and subsequent deactivation of the catalyst [28,29]. Although it was shown that initial oxidative addition of the aldehyde occurred to give a POP-Ph-containing complex *mer*-[Rh(COCH$_2$CH$_2$SMe)(H)(κ^3-P,O,P-POP-Ph)][BAr^F_4] (Ar^F = 3,5-$C_6H_3(CF_3)_2$) (**9**), this complex showed no onward reaction with the alkene, methyl acrylate, at 10 mol% catalyst loading (Scheme 5). Interest-

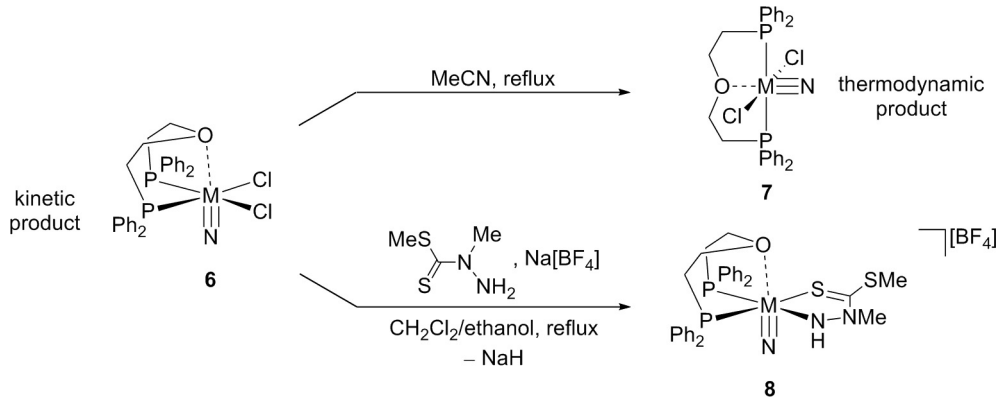

Scheme 3. Irreversible *fac*-κ^3-P,O,P to *mer*-κ^3-P,O,P isomerisation shown by Duatti and co-workers, and the further reactivity of *fac*-isomer **6**. M = Tc, Re.

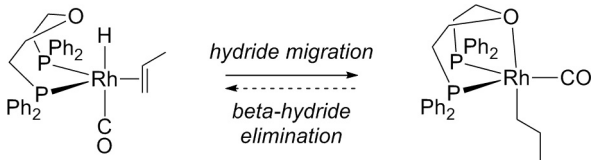

Scheme 4. Proposed ability for the POP-Ph ligand to act as a hemilabile ligand to suppress unwanted *beta*-hydride-elimination events during hydroformylation catalysis.

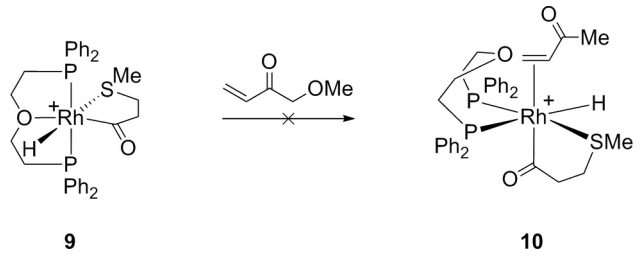

Scheme 5. The inability of the *mer*-κ^3-P,O,P-Ph ether linker to dissociate from the rhodium metal centre during hydroacylation catalysis.

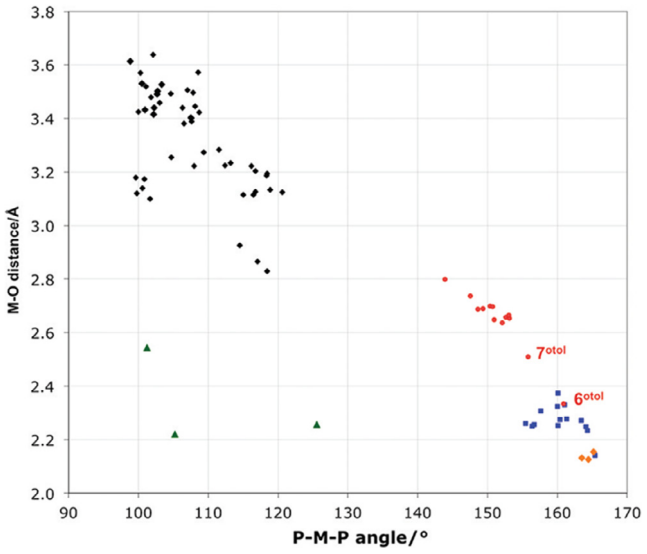

Fig. 3. Plot of M—O distance (Å) versus P—M—P bond angle (°) of {M(Xantphos-Ph)} complexes by Haynes and co-workers (M = transition metal). Reprinted with permission from G.L. Williams, C.M. Parks, C.R. Smith, H. Adams, A. Haynes, A.J.H. M. Meijer, G.J. Sunley, S. Gaemers, Organometallics 30 (2011) 6166–6179. Copyright 2011 American Chemical Society.

ingly, the Xantphos-Ph analogue also showed the same reactivity profile. This was postulated to be due to the unavailability of a vacant site on the metal due to the strong binding of the ether linker of POP-Ph in complex **9** (Rh—O = 2.302(1) Å, P—Rh—P = 156.21(2)°), and hence conversion to the alkene-bound intermediate necessary for onward hydroacylation, *cis*-[Rh(H)(η^2-H$_2$C=CHCOOMe)(MeSCH$_2$CH$_2$CO)(κ^2-P,P-POP-Ph)][BAr$^F_4$] (**10**), was not achieved. This behaviour of POP-Ph contrasted van Leeuwen's Rh-system used for closely related hydroformylation, which did turnover in catalysis (Scheme 4) [26]. Weller's system thus appears to exhibit stronger binding of the POP-Ph ligand, and in particular of the binding of the ether linker through *mer*-κ^3-P,O,P-coordination, compared to the hemilabile *fac*-κ^3-P,O,P-POP-Ph ligand proposed in van Leeuwen's work. The difference in reactivity between *fac* and *mer*-isomers had been presented previously by Duatti [25], and also has relevance for catalysis which involved Xantphos-Ph and DPE-phos ligands as described in Schemes 17 and 30 respectively [30,31].

3. Xantphos-type ligands with aryl substituents

The Xantphos-Ph ligand (4,5-bis(diphenylphosphino)-9,9-dimethylxanthene) was contemporaneously reported in 1995 by the groups of Haenel [32] and van Leeuwen [12]. Other ligands based on the xanthene backbone, also containing diarylphosphine groups and an ether linker, namely Sixantphos (4,6-bis(diphenylphosphino)-10,10-dimethylphenoxasilin) and Thixantphos (2,8-dimethyl-4,6-bis(diphenylphosphino)phenoxathiin), have also been detailed [12]. These ligand types were originally designed to provide bidentate binding to rhodium-based catalysts with varying bite angles for use in hydroformylation catalysis [12]. Whilst in this initial study no hemilabile character of the ligands was reported, nor any sign of ether binding to the metal centre observed, it was shown that increasing the bite angle from Sixantphos (108.7°) to Xantphos (111.7°) gave improved selectivity for linear versus branched aldehyde products – showing possible advantages for their use in catalysis. The potential hemilabile, or at least variable, coordination mode of Xantphos-Ph was largely overlooked until recently. In 2011, Haynes and co-workers presented a survey of crystallographically characterised Xantphos-Ph complexes, and plotted the values of M—O distance (Å) versus P—M—P bite angle (°) (Fig. 3), which elegantly showed, graphically, the wide range of bite angles and coordination modes available to the Xantphos-Ph ligand [33].

An early example of Xantphos-Ph acting as a κ^3-P,O,P pincer-like ligand came from Sandee et al., who immobilised a rhodium complex containing the Xantphos-based ligand, Siloxantphos

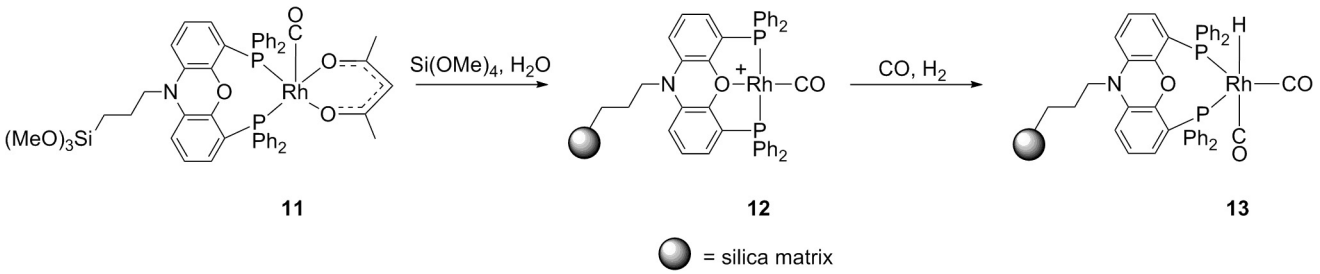

Scheme 6. The immobilisation of a hydroformylation catalyst containing the Siloxantphos ligand using the sol–gel technique.

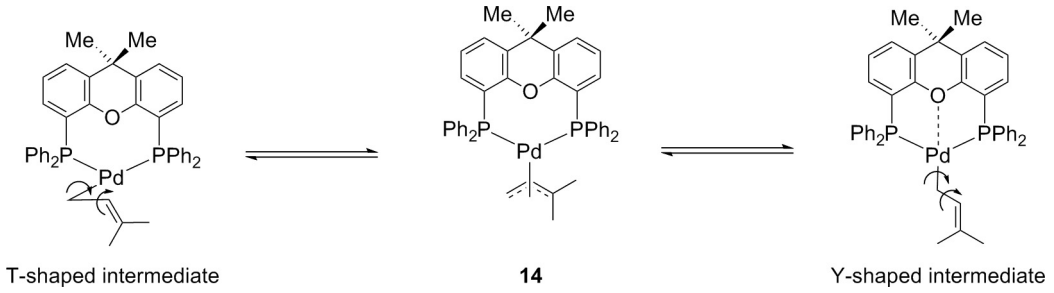

Scheme 7. Proposed intermediates for the π–σ rearrangement in Pd(η^3-1,1-$(CH_3)_2C_3H_3$)(κ^2-P,P-Xantphos-Ph).

(*N*-(3-trimethoxysilane-*n*-propyl)-4,5-bis(diphenylphosphanyl)-phenoxazine), onto a silicate matrix *via* sol–gel synthesis (Scheme 6), for use as a heterogeneous catalyst in hydroformylation [34]. Due to the problems associated with characterisation of this supported catalyst, a model complex containing an unsupported Xantphos-Ph ligand was also exposed to the sol–gel process, but its relative mobility allowed for NMR characterisation in the sol–gel as well as independent single crystal X-ray analysis. During the sol–gel process, the *cis*-Rh(acac)(CO)(κ^2-P,P-Xantphos-Ph) (Siloxantphos analogue = **11**) precursor complex was transformed to the cationic species, *mer*-[Rh(CO)(κ^3-P,O,P-Xantphos-Ph)]$^+$ (Siloxantphos analogue = **12**), the structure of which was confirmed by X-ray crystallography (Rh—O = 2.126 (3) Å, P—Rh—P = 164.42(4)°). On further reaction with CO/H_2, a κ^2-P,P-ligated structure, *cis*-$Rh(CO)_2(H)$(κ^2-P,P-Xantphos-Ph) (Siloxantphos analogue = **13**), was formed, which is a catalyst precursor in hydroformylation [12]. The authors suggested that the κ^3-P,O,P-chelating nature of Xantphos-Ph, and by analogy, Siloxantphos, stabilised the complex during the sol–gel process (Scheme 6), with the hemilability of the ether oxygen allowing the catalytic site to function in the silicate matrix. No comment was made about the change in overall charge between **12** and **13** but it is likely that in such a sol–gel matrix deprotonation of a, rather acidic, bound dihydrogen ligand is possible [35].

The potential for variable interaction between the Xantphos-Ph ether group and a transition metal was also postulated to be important in allyl-palladium complexes reported by van Haaren et al. that showed fluxional behaviour [36]. A π–σ rearrangement was proposed to be responsible for exchange of the *endo* and *exo* forms of *cis*-Pd(η^3-1,1-$(CH_3)_2C_3H_3$)(κ^2-P,P-Xantphos-Ph) (**14**), which could not be frozen out at low temperatures. Two intermediates for the rearrangement were proposed, a T-shaped intermediate and a Y-shaped intermediate which contained a stabilising Pd—O interaction (Scheme 7).

Hartwig and co-workers noted that the Xantphos-Ph CMe_2 groups showed as a single resonance in the ^{1}H NMR spectrum of *cis*-Pd(Cl)(η^3-allyl)(κ^2-P,P-Xantphos-Ph), and proposed that one explanation for the interconversion of the methyl groups was through reversible dissociation of one of the phosphine arms of Xantphos-Ph, which presumably led to transient κ^1-P-coordination of the ligand and subsequent rearrangement of the 3-coordinate intermediate [37]. κ^1-P-bound Xantphos-Ph ligands have also been proposed from DFT calculations of various catalytic transformations (*vide infra*). An even more unusual binding mode of Xantphos-Ph was proposed by Momeni et al. [38], where κ^1-O-binding through the Xantphos-Ph oxygen was postulated to form the 5-coordinate complex $Sn(Me)_2(Cl)_2$ (κ^1-O-Xantphos-Ph) in $CDCl_3$ solution. The ^{1}H NMR spectrum of the complex indicated penta-coordinate geometry of ligands around the tin centre, whilst the ^{31}P NMR spectrum showed a single resonance very close in chemical shift to that of free Xantphos-Ph; which led the authors to suggest that the ligands are unlikely to be bound through either of the phosphine moieties.

The Weller group reported upon iridium complexes of Xantphos-Ph, and found that different coordination modes of the ligand could be obtained [39]. When *cis*-[Ir(COD)(κ^2-P,P-Xantphos-Ph)][BAr^F_4] (COD = 1,5-cyclooctadiene) (**15**) was hydrogenated in CD_2Cl_2 solvent, the bimetallic complex, *fac*-[Ir(H)(μ-H)(κ^3-P,O,P-Xantphos-Ph)]$_2$[BAr^F_4]$_2$ (**16**) formed, however when the analogous reaction was carried out in acetone, monomeric *mer*-[Ir(H)$_2$($OCMe_2$)(κ^3-P,O,P-Xantphos-Ph)][BAr^F_4] (**17**) resulted (Scheme 8). Addition of MeCN to the bimetallic species (**16**) broke up the dimeric structure, resulting in *mer*-[Ir(H)$_2$(NCMe)(κ^3-P,O,P-Xantphos-Ph)][BAr^F_4] (**18**). This reaction was thought to proceed *via* substitution of the bound oxygen at the metal centre of the Xantphos-Ph ligand with acetonitrile, to give another bimetallic species only with *cis*-κ^2-P,P coordination of the Xantphos-Ph ligand, before it dissociated to the corresponding *mer*-κ^3-P,O,P monomers.

P—C and B—H bond activation in stanna-*closo*-borate complexes of {Pd(Xantphos)}$^+$ resulted in the observation of κ^1-P, κ^2-P,P and κ^3-P,O,P-coordination modes of the Xantphos-Ph ligand [40]. The solid-state structure of *mer*-Pd($SnB_{11}H_{11}$)(κ^3-P,O,P-Xantphos-Ph) (**19**, Scheme 9), which was prepared by low temperature recrystallisation from a CH_2Cl_2/Et_2O solution, showed a Pd—O bond (2.171(2) Å). On dissolution in DMF, a dinuclear complex formed, *cis*-$Pd_2(SnB_{11}H_{10})(C_{33}H_{27}P_2O)$($\kappa^2$-P,P-Xantphos) (**20**), in which

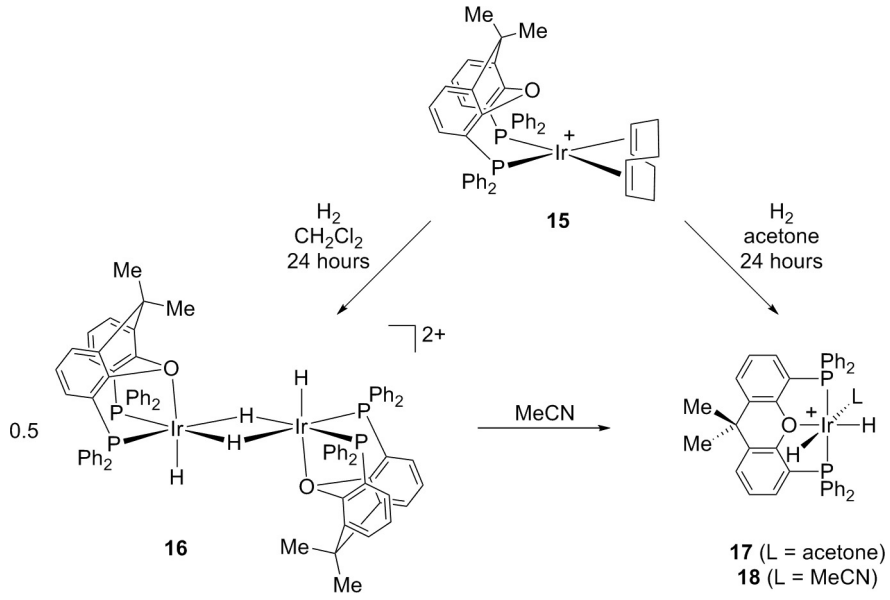

Scheme 8. Weller's cationic {Ir(Xantphos-Ph)} complexes which show differing coordination modes depending on the conditions. BAr^F_4 anions omitted for clarity.

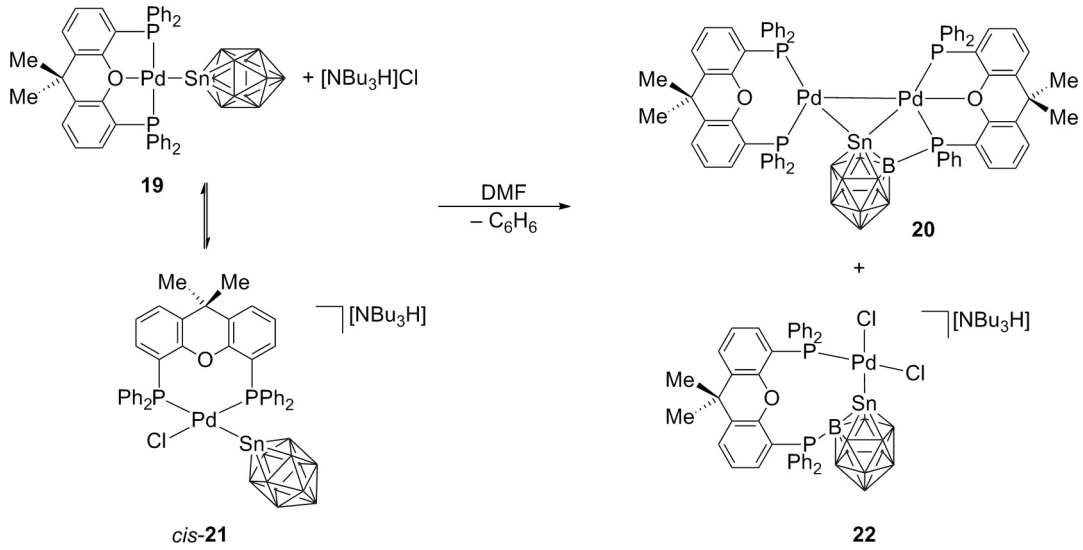

Scheme 9. Palladium complexes of stanna-*closo*-dodecaborate, showed κ^3-P,O,P, κ^2-P,P and κ^1-P-bound Xantphos-Ph, and the equilibrium between the κ^3-P,O,P and κ^2-P,P-complexes **19** and **21**. Unlabelled vertex = B–H.

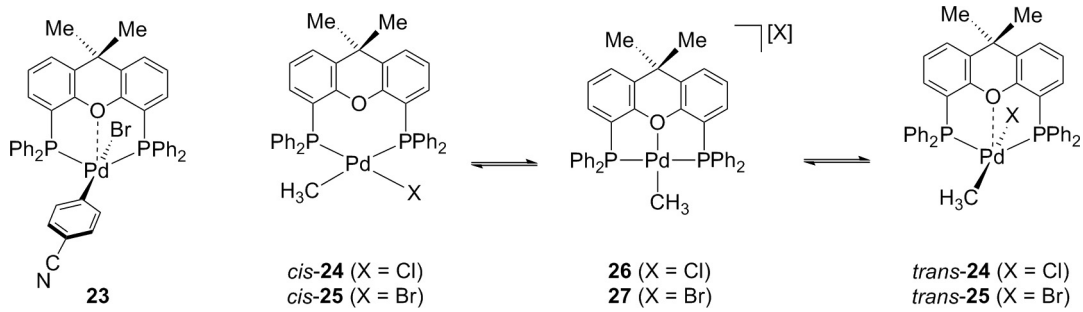

Scheme 10. Left: Structure of complex **23** which is *trans*-κ^2-P,P-bound in the solid-state. Right: Postulated mechanism for *cis*–*trans* isomerisation of $Pd(CH_3)(X)(\kappa^2_{P,P}$-Xantphos-Ph) (X = Cl, Br) *via* a κ^3-P,O,P-Xantphos-Ph cationic intermediate.

one of the PPh groups of the Xantphos-Ph ligand had P—C and B—H activation, with loss of benzene. The P—C activated Xantphos-Ph ligand was shown to coordinate to the metal in a κ^3-P,O,P-orientation, with a short Pd—O bond length (2.234(2) Å). The reaction was also carried out in the presence of $[NBu_3H]Cl$, which showed that the κ^3-P,O,P-bound complex **19** was in equilibrium with a κ^2-P,P-bound complex $[Pd(Cl)(SnB_{11}H_{11})(\kappa^2\text{-P,P-Xantphos-Ph})][NBu_3H]$ (**21**) which exists in both *cis* and *trans* forms. This mixture over time formed the bimetallic $Pd_2(SnB_{11}H_{10})(C_{33}H_{27}P_2O)(\kappa^2\text{-P,P-Xantphos})$ complex **20**, as well as a new mononuclear complex containing a Xantphos-Ph ligand κ^1-P-bound to palladium (complex **22**), in which the free phosphine arm had undergone P—B bond formation with the stanna-*closo*-dodecaborate cage (Scheme 9).

A report by Zuideveld et al. detailed the solution-phase *cis–trans* isomerisation of square planar $Pd(p\text{-}C_6H_4(CN))(Br)(L)$ complexes (L = Xantphos-Ph, Sixantphos and Thixantphos) [41]. The solution room temperature ^{31}P NMR spectra for each complex showed a broad singlet, which resolved into two resonances on cooling to −40 °C, indicating a rapid equilibrium between the *cis* and *trans*-isomers, with the *trans*-isomer favoured at low temperature. Recrystallisation, however, favoured *trans*-$Pd(p\text{-}C_6H_4(CN))(Br)(\kappa^2\text{-P,P-L})$ (e.g., **23**, Scheme 10), and this isomer could be crystallographically characterised for each ligand. Single crystal X-ray diffraction data for *trans*-$Pd(p\text{-}C_6H_4(CN))(Br)(\kappa^2\text{-P,P-Xantphos-Ph})$ (**23**) showed *trans*-coordination of the ligand to the metal centre, with a large P—Pd—P bite angle of 150.35(3)°. Interestingly a weak, at best, Pd···O interaction, 2.698(2) Å, was present, as evidenced by a close to square planar geometry of the complex. The authors suggested that this extra Pd···O interaction between the metal and the Xantphos-Ph ligand may be a factor in stabilising the *trans*-isomer over the *cis*. For the complexes $Pd(CH_3)(Cl)(\kappa^2\text{-P,P-Xantphos-Ph})$ (**24**) and $Pd(CH_3)(Br)(\kappa^2\text{-P,P-Xantphos-Ph})$ (**25**), *cis* and *trans*-isomers were also found to be fluxional at room temperature, but static at −60 °C, and despite being neutral complexes, showed high conductivity values. The authors postulated that this observation may be due to an ionic intermediate, such as *mer*-$[Pd(CH_3)(\kappa^3\text{-P,O,P-Xantphos-Ph})][X]$ (X = Cl (**26**), X = Br (**27**)), that forms during the *cis–trans* isomerisation pathway, which occurs through coordination of the Xantphos-Ph oxygen to palladium, with chloride or bromide dissociation (Scheme 10). It was also noted that the rate of interconversion between the isomers was increased in polar solvents, which would allow further stabilisation of the proposed ionic intermediate which contains a κ^3-P,O,P-Xantphos-Ph ligand.

Other palladium complexes of Xantphos-Ph have been demonstrated to show *cis–trans* isomerisation. For example $[Pd(PPh_2Py)(Xantphos\text{-}Ph)][OTf]_2$, which has a potentially bidentate phosphino-pyridine ligand, displayed fluxional behaviour in solution [42]. Two isomers were observed at −40 °C, which were assigned as *cis*-$[Pd(\kappa^2\text{-N,P-}PPh_2Py)(\kappa^2\text{-P,P-Xantphos-Ph})][OTf]_2$ (**28**) and *mer*-$[Pd(\kappa^1\text{-P-}PPh_2Py)(\kappa^3\text{-P,O,P-Xantphos-Ph})][OTf]_2$ (**29**) (Scheme 11). The mechanism of isomerisation was proposed to

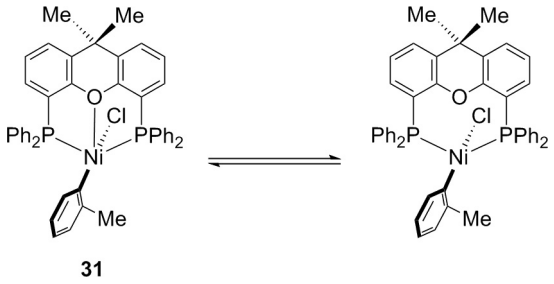

31

Scheme 12. The postulated hemilabile nature of the Xantphos-Ph ether linker in *trans*-$Ni(o\text{-}C_6H_4(CH_3))(Cl)(\kappa^3\text{-P,O,P-Xantphos-Ph})$.

operate through coordination of the Xantphos-Ph ether group with simultaneous decoordination of the pyridine ligand. In this example, both the Xantphos-Ph ligand and the 2-diphenylphosphinopyridine ligand displayed hemilabile character. Whilst neither of these complexes could be characterised using X-ray crystallography, the Pt analogue of complex **29**, *mer*-$[Pt(\kappa^1\text{-P-}PPh_2Py)(\kappa^3\text{-P,O,P-Xantphos-Ph})][OTf]_2$ (**30**), could be studied in the solid-state, which confirmed the presence of a Pt—O bond (2.1889(18) Å) and P—Pt—P bite angle (162.22(2)°) consistent with *mer*-κ^3-P,O,P coordination of the ligand. Interestingly, there was no exchange between the *cis* and *trans*-isomers of the platinum complexes over the same temperature range used for palladium, likely due to the greater metal–ligand bond strengths in Pt complexes versus Pd.

Jamison and co-workers also observed an isomerisation process in their study of air-stable nickel complexes which contained the Xantphos-Ph ligand [43]. The solid-state structure of *trans*-$Ni(o\text{-}C_6H_4(CH_3))(Cl)(Xantphos\text{-}Ph)$ (**31**, Scheme 12) showed a structure that was described as a distorted square pyramidal geometry in the solid-state, but had a rather long apical Ni—O distance (2.5408(6) Å), and a large P—Ni—P bite angle (156.01(1)°), which suggested *trans* orientation of the phosphine groups. In solution, however, the authors observed another isomer by NMR spectroscopy, which they speculated to be the analogous complex which lacked oxygen coordination of the Xantphos-Ph ligand at nickel, shown in Scheme 12, hence suggesting hemilability. It is interesting to note that interconversion of simple rotamers of the *o*-tolyl group in which the methyl was *syn* or *anti* (as suggested crystallographically) to the Xantphos ligand would also provide similar data to those reported.

A common theme of Xantphos-Ph complexes is their ability to promote reductive elimination at transition metal centres [4]. Buchwald noted that the *trans*-$Pd(p\text{-}C_6H_4(CN))(Br)(\kappa^2\text{-P,P-Xantphos-Ph})$ complex, which was contemporaneously prepared by van Leeuwen and co-workers [41], (complex **23**, Scheme 10) (containing a large P—Pd—P angle of 150.70(6)° and weak at best interaction between the palladium and oxygen atoms with a distance of 2.696(4) Å) was a competent catalyst for the amidation of 4-bromobenzonitrile with benzamide [44]. Given that

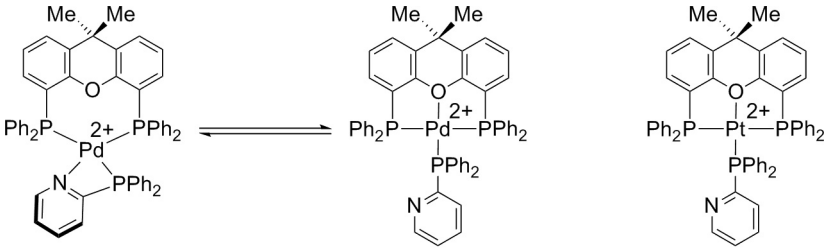

28 **29** **30**

Scheme 11. Left: Postulated mechanism for the *cis*-κ^2-P,P/*mer*-κ^3-P,O,P isomerisation of $[Pd(PPh_2Py)(Xantphos\text{-}Ph)][OTf]_2$. Right: κ^3-P,O,P-Xantphos-Ph complex in the solid-state for **30**. OTf anions omitted for clarity.

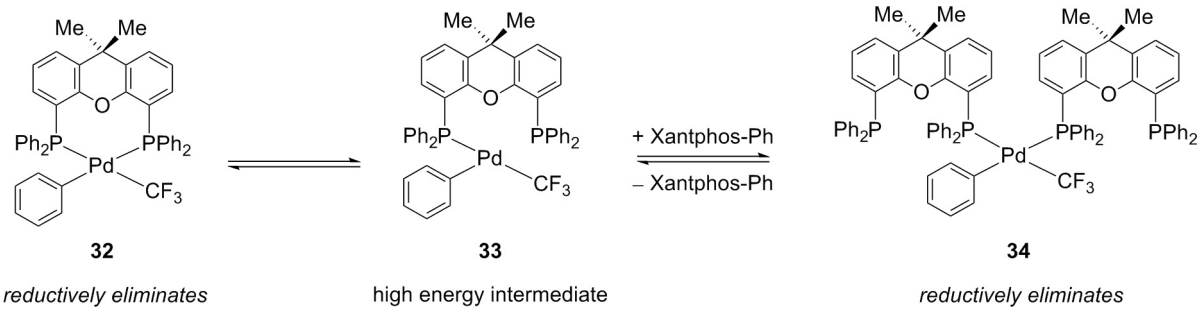

Scheme 13. Possible structures of intermediates from which reductive elimination of Ar–CF_3 could occur from in {Pd(Xantphos-Ph)} complexes. Reductive elimination from **33** was found to be energetically disfavoured.

the aryl halide precatalyst **23** was predominantly *trans* in solution, it was postulated that the proposed intermediate prior to reductive elimination, Pd(*p*-C_6H_4(CN))(NHCOPh)(κ^2-P,P-Xantphos-Ph), would also be *trans*, and therefore that dissociation of one of the phosphine arms could take place to allow reductive elimination from the tricoordinate {Pd(κ^1-P-Xantphos-Ph)} fragment (similar to **33**, Scheme 13), or alternatively, that isomerisation to the *cis*-isomer could occur *via* breaking of the Pd—O interaction and subsequent rearrangement of the phosphine groups. A possible low coordinate κ^1-P-Xantphos-Ph intermediate from which reductive elimination may occur was postulated in later work by Stockland and co-workers who suggested that fast reductive elimination observed during the formation of methylphosphonates using a palladium/Xantphos-Ph system could be due to the dissociation of one of the Xantphos-Ph phosphines immediately prior to reductive elimination, analogous to that of complex **33** (Scheme 13) [45].

Following on from Grushin's initial report on facile Ar—CF_3 bond formation from the corresponding *cis*-κ^2-P,P-Xantphos-Ph complexes of palladium [46], in which the flexible nature of Xantphos-Ph was suggested to be critical, a more detailed study was undertaken in 2012 by Bakhmutov, Grushin, Macgregor and co-workers [47]. Pd(Ph)(CF_3)(κ^2-P,P-Xantphos-Ph) (**32**) was found to be predominantly *cis* in solution, and evidence from both experimental and computational studies suggested that reductive elimination occurred directly from this isomer without the need for breaking of one of the Pd—P bonds, that would result in a higher energy 3-coordinate κ^1-P-Xantphos-Ph complex (**33**) (Scheme 13). Interestingly, when excess Xantphos-Ph was present, the rate of reductive elimination decreased slightly but this effect plateaued at higher ratios of free Xantphos compared to the palladium complex. This was accounted for by the formation of *cis*-Pd(Ph)(CF_3)(κ^1-P-Xantphos-Ph)$_2$ (**34**) – where two Xantphos-Ph ligands bind to the metal by one phosphine arm each – from which reductive elimination could also take place with a relatively low energetic barrier (Scheme 13). This finding suggested that the chelating nature of Xantphos-Ph, with its wide bite angle, is not necessarily required for reductive elimination and monodentate ligands with a steric profile that allows for both *cis*-coordination but remain bulky enough to promote reductive elimination may also be competent ligands for such processes.

A kinetic study on the palladium-catalysed amination of aryl triflates and aryl bromides was reported by van Leeuwen and co-workers, and utilised Xantphos-Ph, DPEphos, Sixantphos, Thixantphos, Thioxantphos and Homoxantphos ligands (L) [48]. Neutral complexes Pd(*p*-C_6H_4(CN))(Br)(L) were synthesised, where the DPEphos and Homoxantphos ligands provided *cis*-κ^2-P,P-coordination to the metal centre only, whilst Sixantphos, Thixantphos and Xantphos-Ph ligands showed *cis*–*trans* isomerisation in solution, with the *trans*-complexes shown to be the crystallographically characterised form (i.e. for *trans*-Pd(*p*-C_6H_4(CN))(Br)(κ^2-P,P-Xantphos-Ph) (*trans*-**23**), see Scheme 10). For these complexes, a weak Pd—O interaction was proposed, with a Pd—O distance of 2.698(2) Å found for complex *trans*-**23** [41]. Only the neutral complexes capable of *cis*–*trans* isomerisation gave appreciable conversions during the amination of bromobenzene, which suggested that the ability of the ligand to adopt different coordination motifs was important. The *cis*/*trans*-Pd(*p*-C_6H_4CN)(Br)(κ^2-P,P-Xantphos-Ph) (*cis*/*trans*-**23**) complex was studied as a precatalyst for this transformation in an in-depth mechanistic study, and the proposed catalytic cycle is detailed in Scheme 14 (only the neutral *cis*-isomer is shown). The pre-equilibrium prior to the rate determining step was controlled by the ability of the Xantphos-type ligand in *cis*-Pd(Ph)(Br)(κ^2-P,P-L) (e.g., **35**) to coordinate the ether oxygen and act in an *associative* hemilabile manner, which triggered dissociation of bromide to form cationic *mer*-[Pd(Ph)(κ^3-P,O,P-L)][Br] (e.g., **36**). For example, the larger bite angle of Xantphos-Ph compared to Sixantphos, resulted in closer proximity between the metal centre and ether oxygen in the Xantphos-Ph complex **35**, which subsequently showed higher reactivity in the amination of aryl bromides relative to the Sixantphos analogue. In comparison, the amination of aryl triflates was achieved by using cationic *trans*-[Pd(*p*-C_6H_4(CN))(κ^3-P,O,P-L)][OTf] complexes (L = Sixantphos, Thixantphos and Xantphos-Ph) as precatalysts. Scheme 14 details the proposed mechanism. In this case, the pre-equilibrium between *trans*-[Pd(Ph)(κ^3-P,O,P-Xantphos-Ph)][OTf] (**37**) and *cis*-[Pd(Ph)(amine)(κ^2-P,P-Xantphos-Ph)][OTf] (**38**), which placed the aryl and the amine *cis*, was proposed to be important – which is influenced by ligand flexibility and bite angle. As Sixantphos has a smaller bite angle than Xantphos-Ph, it favours *cis*-coordination geometry (i.e. **38**) more so than Xantphos-Ph and thus showed greater reactivity in the amination of aryl triflates. These observations demonstrate the subtle interplay between ligand geometries, substrate binding and turnover limiting steps.

The work carried out by Bakhmutov et al. [47], in which excess Xantphos-Ph was found to cause only a slight decrease in the rate of reaction of reductive elimination in palladium complexes was detailed earlier in Scheme 13. However, Eisenburg and co-workers in their study of {Ir(Xantphos-Ph)}-catalysed hydroformylation of 1-hexene [49] found that excess Xantphos-Ph caused deactivation of the catalyst. They also postulated that a κ^2-P,P to κ^1-P-coordination mode change (Scheme 15) may be important for the oxidative addition of dihydrogen during the hydroformylation process. The mechanism for the oxidative addition of H_2 to (crystallographically characterised) Ir(Cl)(CO)$_2$(κ^2-P,P-Xantphos-Ph) (**39**) that results in *cis*-Ir(Cl)(CO)(H)$_2$(κ^2-P,P-Xantphos-Ph) (**40**) was proposed to occur by the steps shown in Scheme 15. No further details of the rate law were obtained.

A study by Macgregor and Grushin in 2014 described the mechanism of the azidocarbonylation of iodobenzene using CO and NaN_3 with an *in situ* formed Pd(CO)$_2$(κ^2-P,P-Xantphos-Ph) precata-

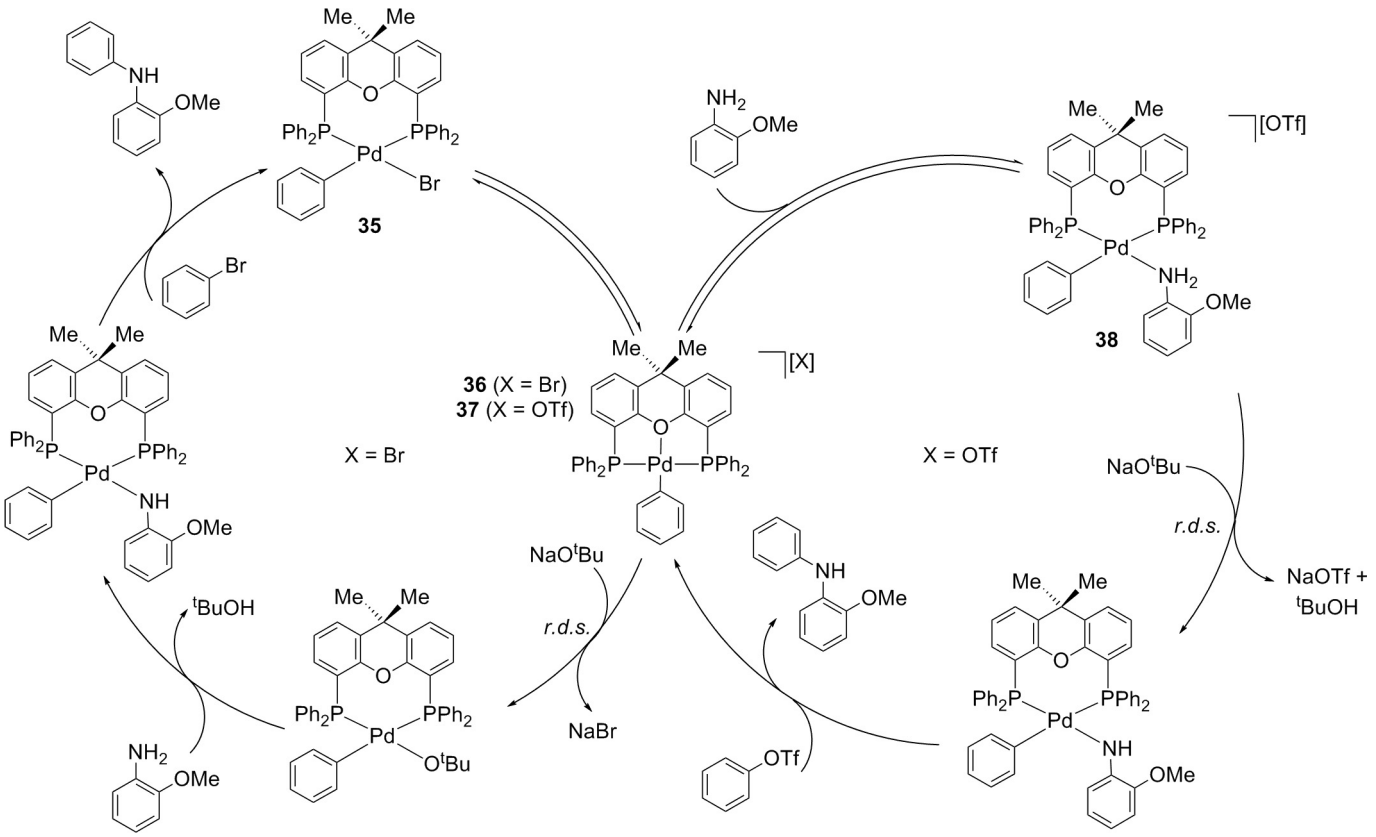

Scheme 14. Catalytic cycles for the amination of aryl bromides and aryl triflates using neutral and cationic {Pd(Xantphos)} complexes respectively.

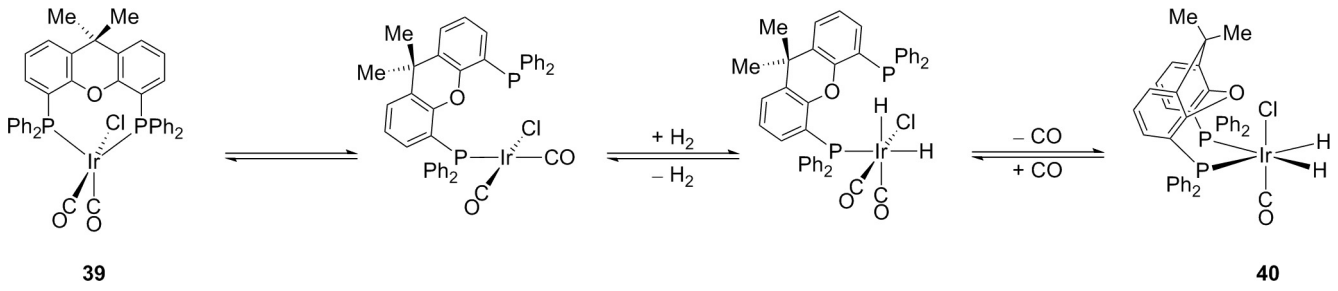

Scheme 15. The proposed dechelation of one of the Xantphos-Ph phosphines to allow the oxidative addition of H_2 at an iridium metal centre.

lyst [50]. They proposed that κ^1-P and κ^2-P,P-Xantphos-Ph species were necessary for the aromatic azidocarbonylation to occur, as one of the phosphine arms must dissociate from the palladium centre to allow oxidative addition of the aryl halide substrate. In 2013, Fu and co-workers proposed, using DFT studies, that the borylation of nitriles using catalysts based upon M(BOR$_2$)(κ^3-P,O,P-Xantphos-Ph) (M = Rh, Ir) required pathways which involved κ^1-P, κ^2-P,P and κ^3-P,O,P-binding of Xantphos-Ph to the metal centre [51]. In contrast, a similar report by Tobisu, Mori and Chatani published a year later, suggested that only κ^2-P,P and κ^3-P,O,P-complexes were required for a similar transformation [52]. In 2016, Slaughter and co-workers calculated that the C—H arylation of binaphthyl triflates could be promoted using a {Pd(Xantphos-Ph)}$^+$ catalyst *via* an inner-sphere concerted metalation–deprotonation (CMD) mechanism, which involved κ^3-P,O,P (**41**), κ^2-P,P (**42**) and κ^1-P-Xantphos-Ph species (**43**) (Scheme 16) [53]. This was found to be the lowest energy pathway, with the other option an outer-sphere CMD arylation pathway in which the ligand remained κ^2-P,P-bound. The ability of the Xantphos-Ph ligand to display hemilabile behaviour therefore enables the inner-sphere mechanism, and the authors also note that the wide angle possessed by Xantphos-Ph was responsible for facile reductive elimination of the helicene product of C—H arylation.

As shown, κ^1-P-binding of the Xantphos-Ph ligand has been a proposed mode of binding in intermediates of catalytic reactions. Whilst such behaviour has been supported by computation, there is no direct experimental evidence for a κ^1-P/κ^2-P,P-coordination mode change in transition metal complexes during catalysis. Isolated examples where Xantphos-Ph binds in a κ^1-P-manner show however that such hemilability is plausible (e.g., complexes **22** and **65**).

The catalytic carbothiolation of phenylacetylene with 2-(methylthio)acetophenone using a *mer*-[Rh(PhCCPh)(κ^3-P,O,P-Xantphos-Ph)][BAr$^F_4$] precatalyst (**44**) was reported by Weller and Willis, in which the Xantphos-Ph ligand is proposed to occupy *cis*-κ^2-P,P, *fac*-κ^3-P,O,P and *mer*-κ^3-P,O,P coordination sites during the catalytic cycle, shown in Scheme 17 [30]. Interestingly, the reaction from the Rh(I) precatalyst (complex **44**) showed two catalytic

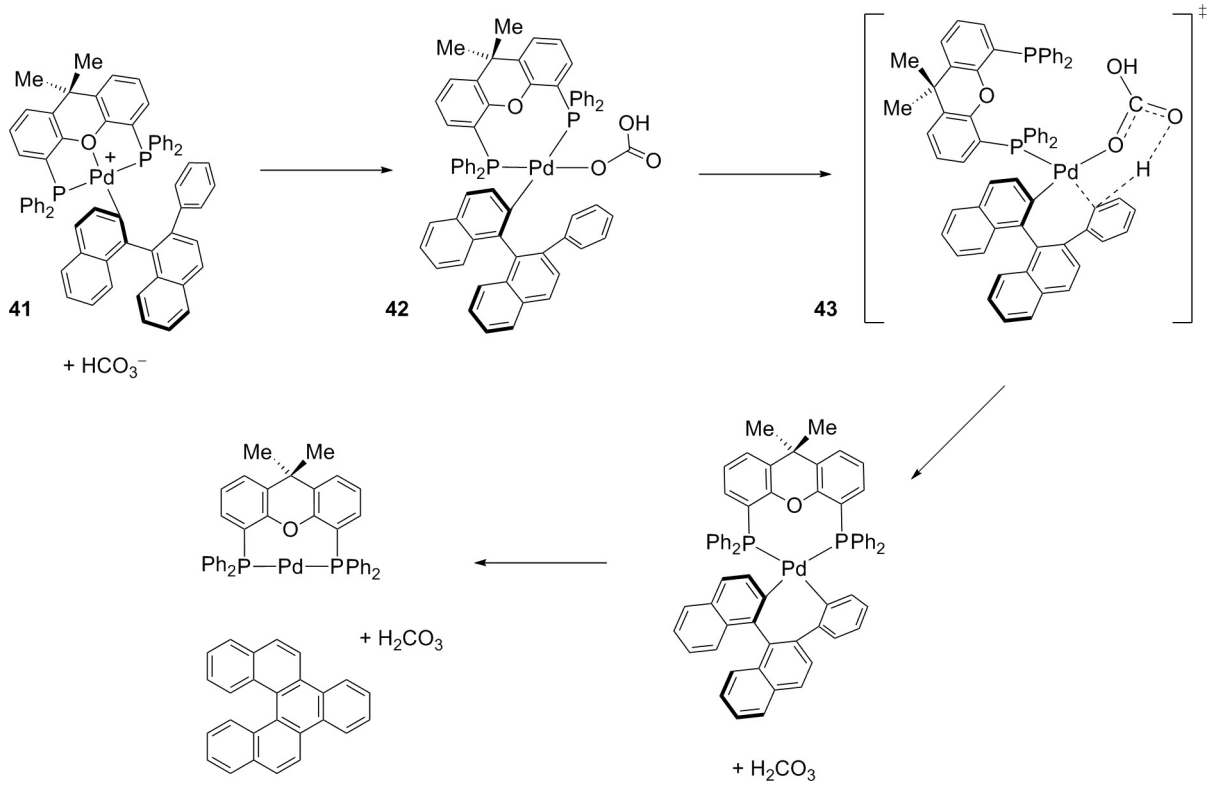

Scheme 16. Selected intermediates and transition states proposed for the inner sphere CMD mechanism calculated by Slaughter and co-workers during C—H arylation catalysis.

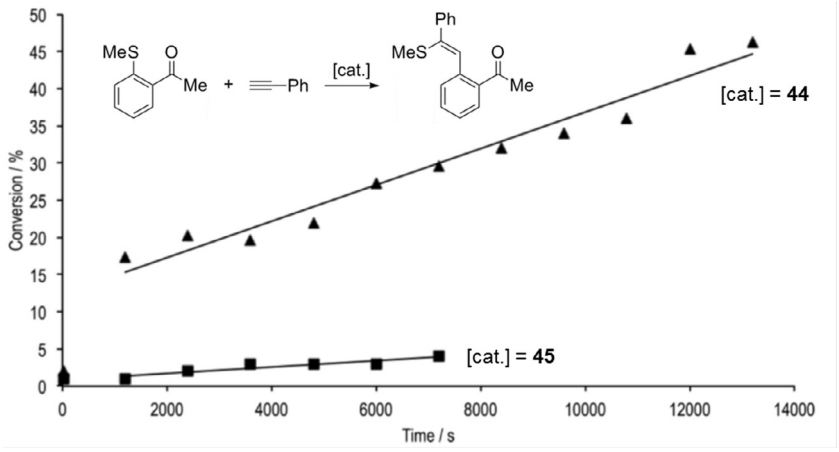

Fig. 4. Conversion versus time plot for the hydroacylation catalysis of complexes **44** and **45**. Reprinted and adapted with permission from P. Ren, S.D. Pike, I. Pernik, A.S. Weller, M.C. Willis, Organometallics 34 (2015) 711–723. Copyright 2015 American Chemical Society.

regimes at 373 K: a fast region that gave 15% conversion after 20 min which was followed by a much slower rate (Fig. 4), suggesting that an initially fast catalyst was formed which then converted to a slower less-active species. The *mer*-Rh(III) aryl sulphide complex (**45**) was the only organometallic species observed in the reaction mixture by $^{31}P\{^{1}H\}$ NMR spectroscopy. This complex could be prepared independently at room temperature as the thermodynamic product of the reaction of the Rh(I) precatalyst **44** with 2-(methylthio)acetophenone after 32 h, which initially formed a 20:1 ratio of *fac*-κ^3-P,O,P and *mer*-κ^3-P,O,P isomers. On heating this mixture to 373 K, full conversion to the thermodynamically favoured *mer*-isomer was achieved after 40 min. The *mer*-κ^3-P,O,P complex (**45**) could be isolated, and its crystallographically-determined structure showed a tridentate pincer geometry of the ligand (P—Rh—P = 165.22(5)°, Rh—O = 2.215(3) Å). The *fac*-κ^3-P,O,P isomer (**46**) could not be structurally characterised. When pure *mer*-κ^3-P,O,P complex **45** was used as the precatalyst the rate of reaction was slow at 373 K, with no fast regime observed (Fig. 4). This suggested that the *mer*-complex was responsible for the later, slow, catalytic regime when starting from Rh(I) precatalyst **44**, and that the kinetically favoured *fac*-κ^3-P,O,P complex **46** was the fast active catalyst. It was proposed that the *fac*-isomer **46** could easily dissociate the ether linkage of the Xantphos-Ph ligand to form *cis*-[Rh(σ,κ^1-O-C_6H_4COMe)(SMe)(κ^2-P,P-Xantphos-Ph)][BAr^F_4] (**47**) which would

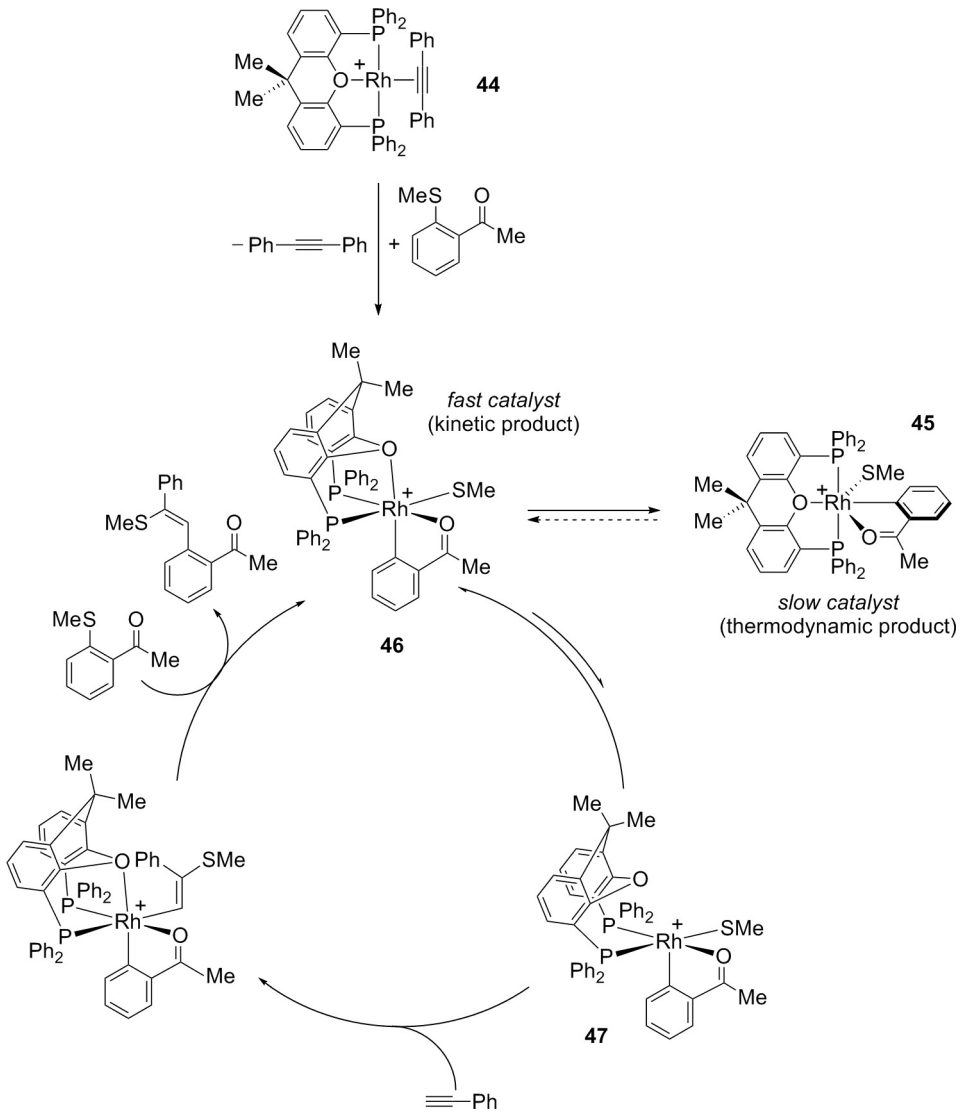

Scheme 17. Proposed catalytic cycle for the catalytic carbothiolation of phenylacetylene using the κ^3-P,O,P-Xantphos-Ph catalyst **44**, *mer*-[Rh(PhCCPh)(κ^3-P,O,P-Xantphos-Ph)][BAr^F_4]. BAr^F_4 anions omitted for clarity.

then allow the alkyne to bind in the appropriate orientation on the metal for subsequent SMe migratory insertion. A similar observation for *fac*-κ^3-P,O,P versus *mer*-κ^3-P,O,P isomers in carbothiolation chemistry had been reported earlier by the same group using the DPEphos ligand (see Scheme 30) [31]. Other *fac*–*mer* isomerisation of Xantphos-Ph complexes were also reported by the Weller group in their study of {Rh(H)$_2$(κ^3-P,O,P-Xantphos-Ph)}$^+$-containing complexes (e.g., see Scheme 25).

The interplay between κ^2-P,P and κ^3-P,O,P-complexes of the Xantphos-Ph ligand as intermediates during catalysis have also been proposed to be important by James and co-workers in the hydrogenolysis of model lignin compounds, e.g., **49** [54], using *cis*-Ru(H)$_2$(CO)(PPh$_3$)(κ^2-P,P-Xantphos-Ph) (**48**), a complex originally reported and crystallographically characterised by Whittlesey and Williams [55]. The ruthenium precatalyst operated on substrate **49** to give both *fac*-κ^3-P,O,P and *mer*-κ^3-P,O,P-Xantphos-Ph complexes (e.g., *mer*-complexes **50** and **51**, Scheme 18) which resulted from overall dehydrogenation or dehydrogenation/hydrogenolysis respectively. Such a requirement for κ^2-P,P/κ^3-P,O,P flexibility was also demonstrated by Johnson et al. in the catalytic dehydrocoupling of amine-boranes [56]. A κ^2-P,P-precatalyst, *cis*-[Rh(η^2-H$_2$B(CH$_2$CH$^t_2$Bu)·NMe$_3$)(κ^2-P,P-Xantphos-Ph)][BAr^F_4] (**52**), initially formed a Rh(III) κ^3-P,O,P-species, *mer*-[Rh(H)$_2$(η^1-H$_3$B·NMeH$_2$)(κ^3-P,O,P-Xantphos-Ph)][BAr^F_4] (**53**) on addition of H$_3$B·NMeH$_2$ as the first step of the dehydrocoupling process (Scheme 18).

Haynes and co-workers proposed a mechanism for methanol carbonylation using {Rh(Xantphos-Ph)}$^+$ complexes in which κ^2-P,P to κ^3-P,O,P-rearrangements in Xantphos are proposed to be important [33]. Whilst throughout the catalytic cycle, the Xantphos-Ph ligand is shown to be predominantly *mer*-κ^3-P,O,P-bound (Scheme 19), the initial oxidative addition of MeI occurs at what is postulated to be a *trans*-κ^2-P,P complex, *trans*-Rh(CO)(I)(κ^2-P,P-Xantphos-Ph) (**54**). Whilst structural data for this Rh(I) complex could not be obtained, the Xantphos-(*o*-tol) analogue of complex **54**, *trans*-Rh(CO)(I)(κ^2-P,P-Xantphos-(*o*-tol)) (**54**-*o*-tol), was crystallographically characterised, which showed the Rh—O distance to be reasonably short (2.334(4) Å). However, they noted that MeI oxidative addition to this complex was disfavoured, possibly due to the increased steric bulk from the *o*-methyl groups, therefore **54**-*o*-tol could not accurately describe the catalytic cycle proposed for Xantphos-Ph. DFT calculations suggested that there was heightened nucleophilicity of complex **54** because the Xantphos-Ph ether oxygen could associatively stabilise the S_N2

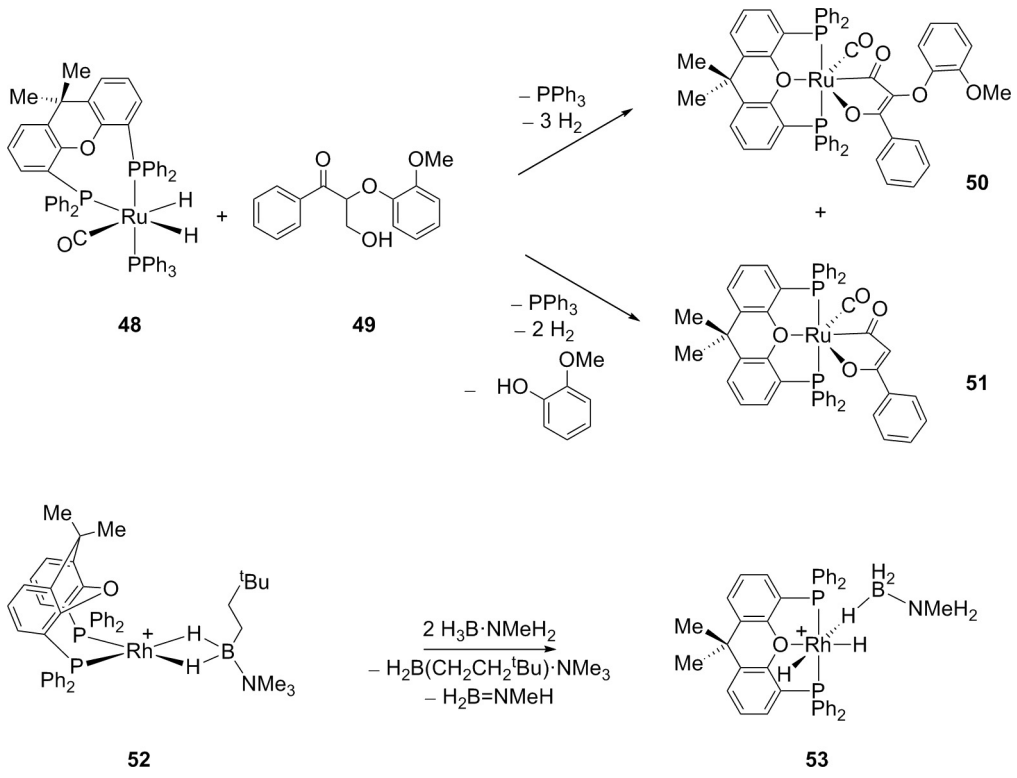

Scheme 18. Top: Dehydrogenation/hydrogenolysis of model lignin structure **49** by {Ru(κ^2-P,P-Xantphos-Ph}. Bottom: Change in coordination mode of the Xantphos-Ph ligand in the first step of $H_3B{\cdot}NMeH_2$ dehydrocoupling. BAr^F_4 anions omitted for clarity.

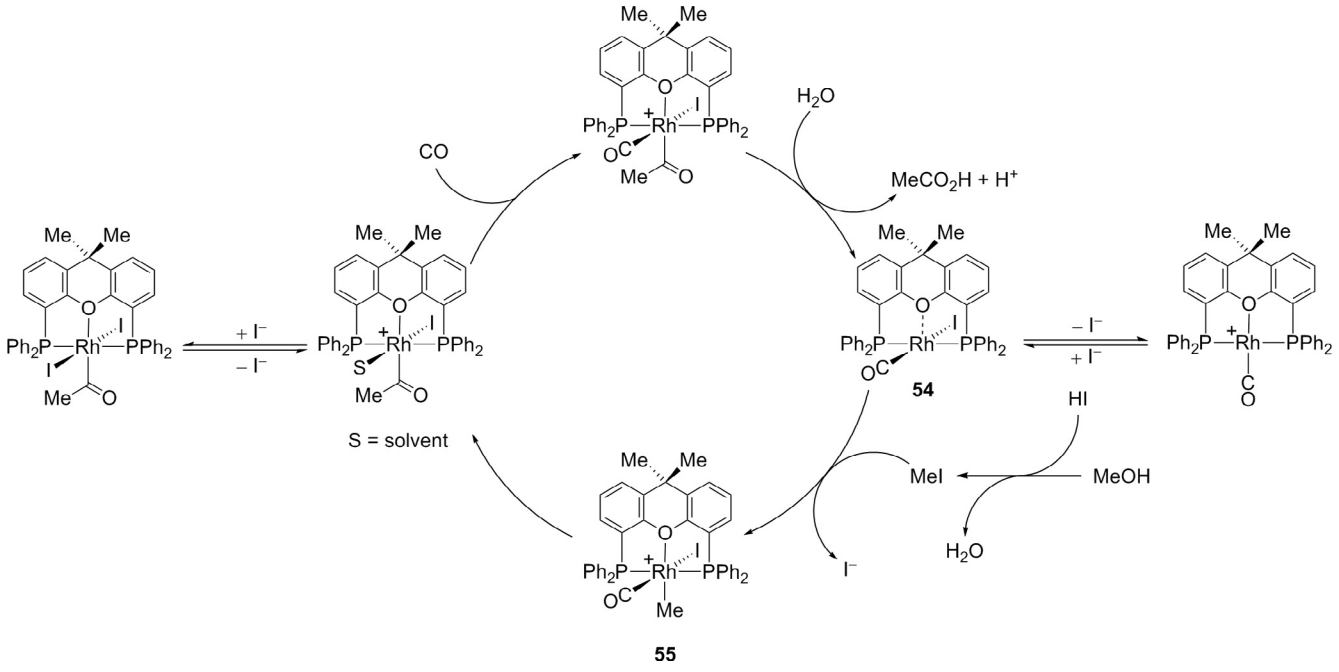

Scheme 19. Proposed catalytic cycle for the carbonylation of methanol using a {Rh(Xantphos-Ph)} species.

transition state of MeI oxidative addition – the product of which was *mer*-[Rh(CO)(I)(Me)(κ^3-P,O,P-Xantphos-Ph)]$^+$ (**55**) – highlighting the important role of the metal–oxygen interaction in promoting reactivity. Given the wide range of bite angles and coordination modes Xantphos-Ph can encounter, as shown by their survey of transition metal Xantphos-Ph complexes (Fig. 3), they also noted that the κ^3-P,O,P-intermediates postulated during the reaction could alternatively adopt *fac*-κ^3-P,O,P geometries instead, although these were not specifically detailed.

4. Xantphos-type ligands with alkyl substituents

In comparison to the Xantphos-Ph parent ligand, which formed Pd(Ph)(CF_3)(κ^2-P,P-Xantphos-Ph) (**32**, Scheme 13) with both *cis*

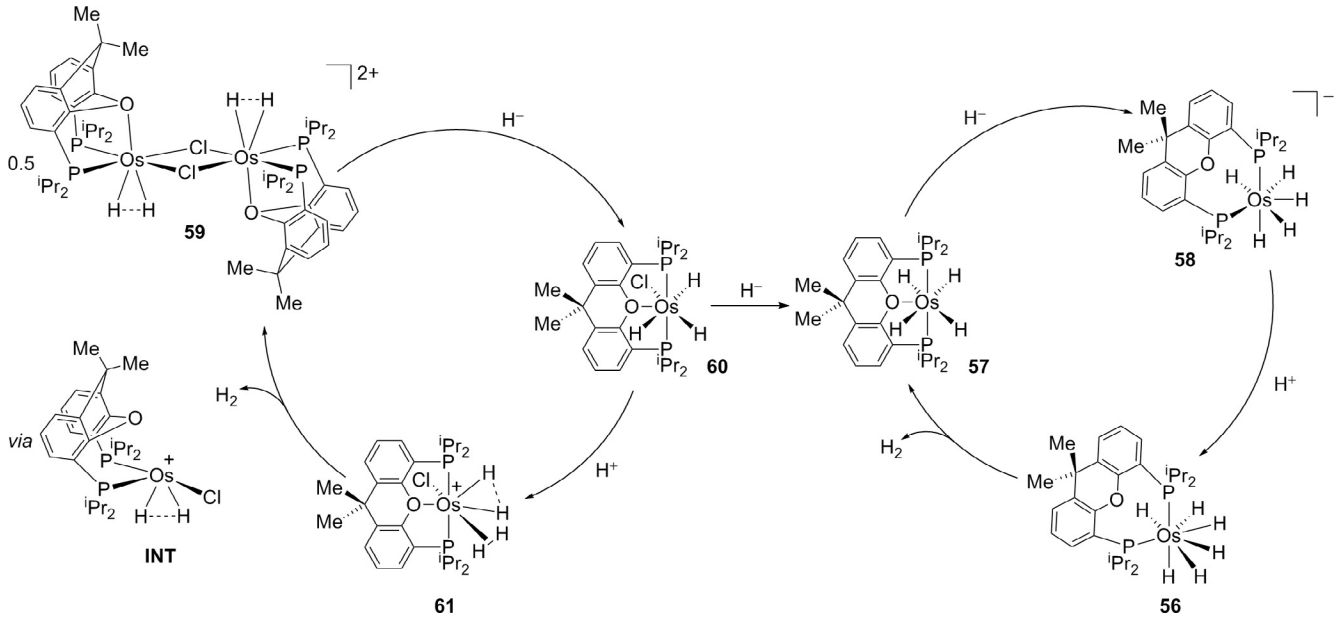

Scheme 20. Variable coordination modes of the Xantphos-^{i}Pr ligand.

and *trans*-isomers observed in solution (the *cis*-isomer is the crystallographically characterised complex), the analogous Xantphos-^{i}Pr complex was found to be exclusively *trans*-κ^2-P,P-bound in both solid-state and in solution [47]. In addition, reductive elimination from *trans*-Pd(Ph)(CF$_3$)(κ^2-P,P-Xantphos-^{i}Pr) was much slower in comparison to the Xantphos-Ph analogue, presumably due to the lower propensity for this complex to form *cis*-complexes required for this process. Whilst the P—Pd—P bond angle was in the range expected for *trans*-coordination of Xantphos-^{i}Pr at the metal centre (144.46(2)°), a possible Pd—O interaction was less likely, as the distance between the two atoms is 2.784(1) Å – much longer than the lengths of Pd—O bonds present in other Xantphos-containing complexes [40,41,57].

The ability of the Xantphos-^{i}Pr to coordinate to a metal centre in both κ^2-P,P and κ^3-P,O,P-fashions has been demonstrated by Esteruelas and co-workers in osmium complexes [58]. The hexahydride complex, *cis*-Os(H)$_6$(κ^2-P,P-Xantphos-^{i}Pr) (**56**, Scheme 20), where the ligand was bound in a *cis*-bidentate manner, was stable in solid form or in solution under an atmosphere of H$_2$. Although the solid-state structure could not be obtained using single crystal X-ray diffraction, the DFT-optimised structure of the complex revealed a P—Os—P angle of 105.4°, a structure consistent with *cis*-κ^2-P,P-Xantphos-^{i}Pr coordination. However, when the hexahydride complex was left in MeOH solution under an argon atmosphere, one equivalent of H$_2$ was lost slowly over time, forming the tetrahydride complex, *mer*-Os(H)$_4$(κ^3-P,O,P-Xantphos-^{i}Pr) (**57**, Scheme 20), where the overall coordination mode switches from *cis*-κ^2-P,P to *mer*-κ^3-P,O,P. The κ^3-P,O,P-ligated complex was characterised by single crystal X-ray crystallography, and showed a short Os—O bond (2.222(3) Å) and a wide P—Os—P angle (164.53(5)°) (data for one of the four crystallographically independent molecules in the asymmetric unit), which confirmed the pincer-like, *mer*-geometry of the ligand.

From this initial work, a wider variety of variable coordination modes of Xantphos-^{i}Pr were reported in 2017, again by the group of Esteruelas [59]. A number of dihydrogen and hydride complexes were stabilised by *cis*-κ^2-P,P, *fac*-κ^3-P,P and *mer*-κ^3-P,O,P binding of this ligand with Os, by stepwise addition of H$^+$ and H$^-$ sources, and overall loss of one equivalent of H$_2$ (Scheme 20). Completion of the cycle which involved H$_2$ loss from complex **56** to form **57** was achieved by hydride addition to **57** to form anionic *cis*-[Os(H)$_5$(κ^2-P,P-Xantphos-^{i}Pr)]$^-$ (**58**) which was characterised by a single crystal X-ray diffraction study. It was noted that *mer*-κ^3-P,O,P-coordination of Xantphos-^{i}Pr appeared to be favoured over *fac*-κ^3-P,O,P in the saturated mononuclear complexes, whilst the only *fac*-κ^3-P,O,P-Xantphos-^{i}Pr complex, *fac*-[(Os(H···H)(μ-Cl)(κ^3-P,O,P-Xantphos-^{i}Pr)$_2$]$^{2+}$ (**59**) reported in this work was shown to be dimeric with bridging halide ligands, similar to that of iridium Xantphos-Ph complexes reported by Weller and co-workers (Scheme 8). Complex **59** was additionally characterised by X-ray diffraction studies. Hydride addition to **59** formed the previously reported *mer*-Os(H)$_3$(Cl)(κ^3-P,O,P-Xantphos-^{i}Pr) (**60**) [58], which when protonated gave, *mer*-[Os(Cl)(H···H)(μ^2-H$_2$)(κ^3-P,O,P-Xantphos-^{i}Pr)]$^+$, complex **61**. The *mer*-κ^3-P,O,P coordination of Xantphos-^{i}Pr in complex **61** was proposed using DFT calculations, and was in full agreement with the analogous *mer*-[Os(Cl)(H···H)(μ^2-H$_2$)(κ^3-P,O,P-DBFphos-^{i}Pr)][BF$_4$] which could be synthesised independently and crystallographically characterised. A very recent study by the same group proposed that H$_2$ loss to form complex **59** from **61** proceeded through *cis*-[(Os(H···H)(Cl)(κ^2-P,P-Xantphos-^{i}Pr)]$^+$ (**INT**, Scheme 20), which could be trapped by HBpin and HBcat to form *neutral mer*-Os(H)(Cl)(η^2-HBpin)(κ^3-P,O,P-Xantphos-^{i}Pr) and *mer*-Os(H)(Cl)(η^2-HBcat)(κ^3-P,O,P-Xantphos-^{i}Pr) respectively [60].

The bulkier Xantphos-^{t}Bu ligand was also shown to adopt both *trans*-κ^2-P,P and *mer*-κ^3-P,O,P-coordination modes with a few crystallographically characterised examples reported, including *mer*-{Rh(κ^3-P,O,P-Xantphos-^{t}Bu)} complexes prepared by Goldman and co-workers in 2013 [61]. In 2016, Sun, Zhang and co-workers synthesised gold complexes of Xantphos-^{t}Bu for use in catalytic C—F to C—X (X = O, S or N) bond transformation studies [62]. Au(Cl)(κ^2-P,P-Xantphos-^{t}Bu) (**62**) was shown to be a tricoordinate complex with κ^2-P,P-coordination of the ligand, where the X-ray diffraction data showed an Au···O distance of 2.866(3) Å and a P—Au—P bond angle of 140.28(4)°. On reaction with GaCl$_3$, *mer*-[Au(κ^3-P,O,P-Xantphos-^{t}Bu)][GaCl$_4$] (**63**) was formed (Scheme 21), leading to a shortening of the Au—O bond distance to 2.625(4) Å and widening of the P—Au—P bond angle to 155.18(6)° – possibly suggestive of a change in ligand binding mode from κ^2-P,P to κ^3-P,O,P – although the Au—O distance is still long. The Au(Cl)(κ^2-P,P-Xantphos-^{t}Bu) catalyst (**62**) was found to carry out a C—F to C—O bond transformation of pentafluoronitrobenzene using

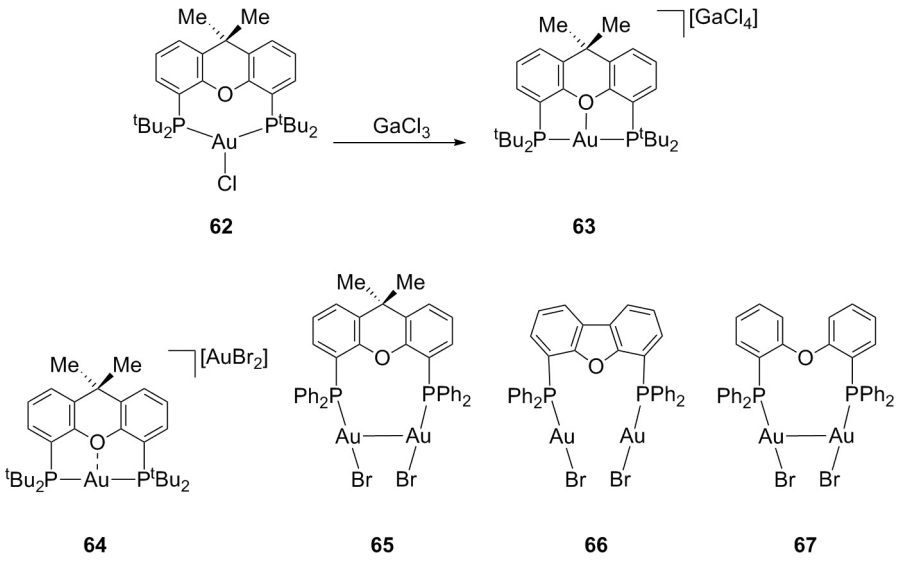

Scheme 21. Examples of gold complexes containing Xantphos-^{t}Bu, Xantphos-Ph, DBFphos and DPEphos.

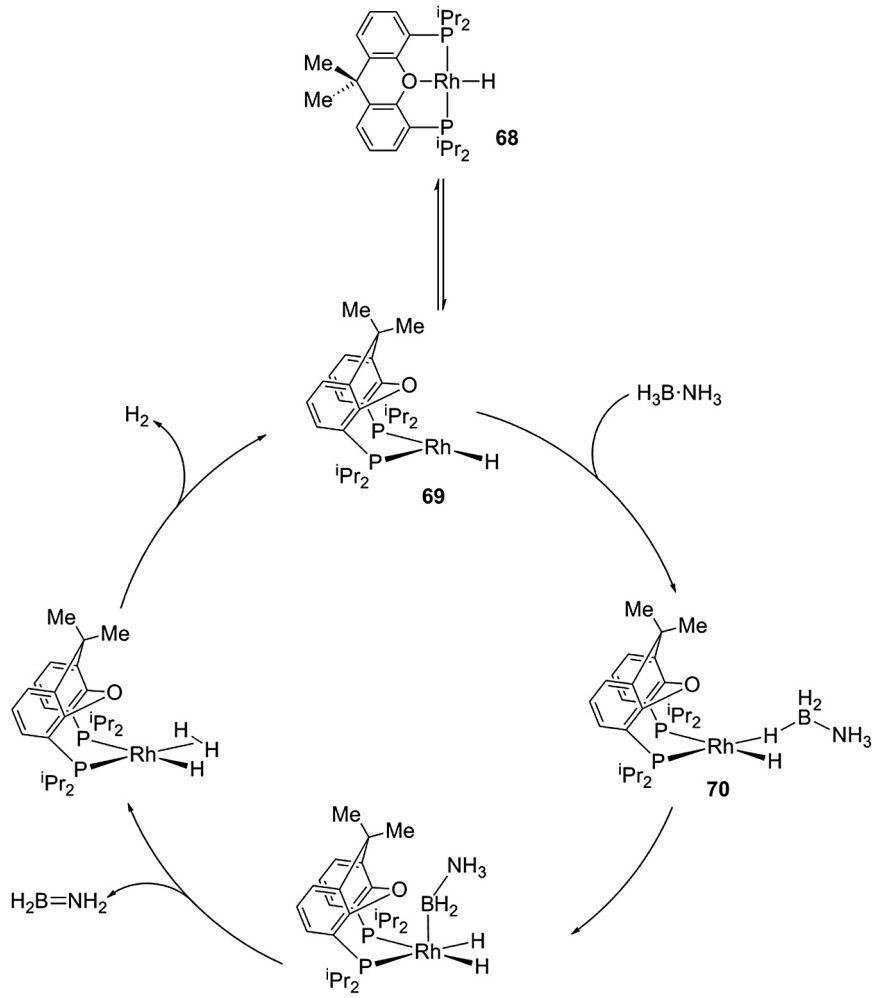

Scheme 22. Calculated catalytic cycles for the dehydrogenation of ammonia borane using *mer*-κ^{3}-P,O,P-Xantphos-^{i}Pr complex **68**.

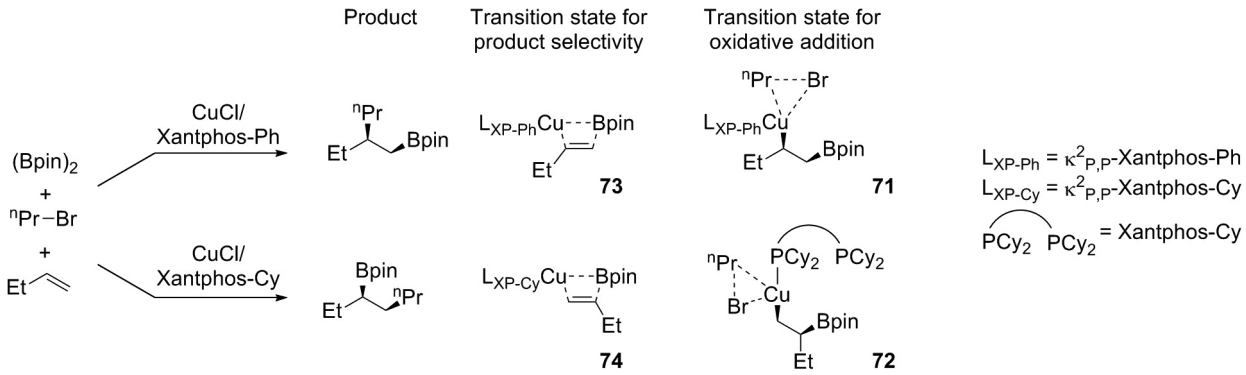

Scheme 23. The difference in identity of the transition states calculated and products formed during alkylboration of 1-butene using Xantphos-Ph and Xantphos-Cy.

methoxytrimethylsilane with increased performance and selectivity compared to its Xantphos-Ph analogue, postulated to be due to the elongated Au—Cl bond in the alkyl Xantphos complex resulting from greater electron donor character of Xantphos-^{t}Bu versus Xantphos-Ph. The *mer*-κ^3-P,O,P binding of Xantphos-^{t}Bu to form a cationic complex was also suggested by Partyka et al. in *mer*-[Au(κ^3-P,O,P-Xantphos-^{t}Bu)][AuX_2] (X = Cl, Br (**64**), I) (Scheme 21) ion pair complexes (Au—O = 2.660(3) Å for X = Br), albeit with a long Au···O distance [63]. Interestingly, with different ligands such as Xantphos-Ph, DBFphos and DPEphos (L), $(AuX)_2$(L) (X = Br, I, whilst X = Cl was reported by Lagunas and co-workers [64]) dimeric gold complexes formed, where the ligand binds in a κ^1-P-manner to each Au atom, as shown in Scheme 21 (e.g., X = Br, L = Xantphos-Ph (**65**), DBFphos (**66**), DPEphos (**67**)). The pincer-type coordination mode observed by the Xantphos-^{t}Bu ligand was proposed to occur due to the greater rigidity of the ligand, combined with the bulky ^{t}Bu groups which did not allow a short enough P–P distance to form within the complex to accommodate a stable Au_2 pair, as occurs for the less sterically bulky Xantphos-Ph, DPEphos and DBFphos ligands.

Esteruelas studied the Xantphos-^{i}Pr ligand in catalytic ammonia borane and dimethylamine-borane dehydrogenation [65]. The pre-catalyst of choice was a neutral *mer*-Rh(H)(κ^3-P,O,P-Xantphos-^{i}Pr) complex (**68**), which DFT calculations showed to dissociate the oxygen atom of the Xantphos-^{i}Pr ligand to form a tricoordinate T-shaped intermediate (**69**) to which the amine–borane could bind to form a sigma-complex (**70**) (Scheme 22). The mechanism suggested showed that the ligand remained *cis*-κ^2-P,P-coordinated to the rhodium centre throughout the catalytic cycle (Scheme 22), although there was no experimental evidence for this reported.

A computational report from Yu and Fu demonstrated that the alkylboration of 1-butene using $(Bpin)_2$ and 1-bromopropane, catalysed by Cu(Bpin)(Xantphos-R) complexes (R = Ph or Cy) operated by a mechanism that diverged at the oxidative addition step of the alkyl halide, the route of which was dependent on the substituent at the Xantphos-R phosphine groups [66]. Whilst Xantphos-Ph remained κ^2-P,P-bound to the metal centre at the rate-determining oxidative addition transition state (**71**), the equivalent complex containing Xantphos-Cy dissociated one of the phosphorus arms to form a κ^1-P-Xantphos-Cy transition state (**72**) (Scheme 23). Interestingly, the use of Xantphos-Cy ligand compared to the Xantphos-Ph also promoted differences in regioselectivity, favouring the Markovnikov and *anti*-Markovnikov products respectively. The authors explained this difference by the comparison of steric bulk of Cy versus Ph – the lower steric bulk of Xantphos-Ph enabled the ethyl substituent to lie close to the Xantphos-Ph ligand in the transition state (**73**) giving the *anti*-Markovnikov product, whereas the Xantphos-Cy ligand favoured the ethyl substituent on the alkene to be closer to the Bpin ligand in the corresponding transition state (**74**), which facilitated Markovnikov-selective alkene insertion.

5. DBFphos-type ligands

The synthesis of DBFphos (4,6-bis(diphenylphosphino)dibenzofuran) was first published in 1991 by Haenel et al. [67], and was found to have a wide natural bite angle of 131.1°, much larger than that of Xantphos-type ligands [12]. Initially, this was proposed to be of use in the stabilisation of bimetallic complexes through κ^1-P-binding of each phosphine to a transition metal centre, for example $Co_2(CO)_6$(κ^1-P,κ^1-P-DBFPhos) (**75**) (Fig. 5) [68]. The authors also discussed the possibility of oxygen coordination from the dibenzofuran motif to one of the cobalt centres, as this may have an effect on the potential catalytic activity of the complex, however the crystal structure indicated that no such Co—O interaction existed, as the distances between each Co and oxygen being long, i.e. 3.345(3) Å or 3.302(2) Å. Similarly, work by the groups of Lagunas [64], and Gray [63], showed that the DPFphos ligand also behaved in a κ^1-P,κ^1-P-binding mode to stabilise Au_2 complexes, $(AuX)_2$(κ^1-P,κ^1-P-DBFphos) where X = Cl, Br, I (e.g., **66**, Scheme 21). Interestingly, for the complexes where X = Cl or Br, an intramolecular aurophilic interaction between the gold atoms was not observed, unlike for Xantphos-Ph analogues (e.g., **65**). This was possibly due to the wide bite angle of the ligand which allowed for intermolecular Au···X stabilising interactions, rather than close, intramolecular Au—Au interactions which are generally considered to be weak. A report by Walton suggested that DBFphos could behave as a κ^1-P-ligand bound to one metal centre only in $[Re_2(Cl)_7(\kappa^1\text{-P-DBFphos})][N^nBu_4]$ (complex **89** shows the analogous DPEphos structure) [69], as evidenced by two separate resonances observed by ^{31}P NMR spectroscopy for the complex, which indicated one phosphine environment was bound to the rhenium metal centre, whereas the second phosphine displayed a chemical shift indicative of the free ligand.

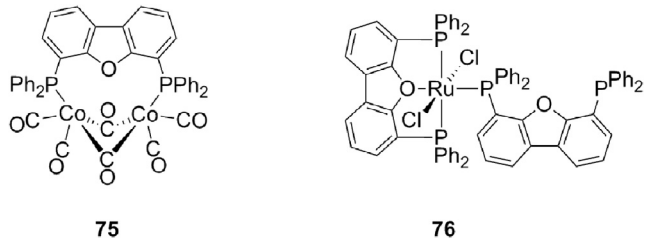

Fig. 5. Examples of different coordination modes of the DBFphos ligand.

Vogl et al. utilised the DBFphos ligand in their synthesis of *mer*-$Ru(Cl)_2(\kappa^1$-P-phosphine$)(\kappa^3$-P,O,P-DBFphos) complexes (κ^1-P-phosphine = DBFphos (**76**), PPh_3, *p*-tol), and found that the DBFphos ligand was surprisingly bound to the metal in both κ^1-P and κ^3-P,O,P-coordination modes in the same molecule (Fig. 5) [70]. Unfortunately, crystals of sufficient quality of complex **76**, $Ru(Cl)_2(\kappa^3$-P,O,P-DBFphos$)(\kappa^1$-P-DBFphos), could not be obtained, therefore a detailed structural analysis of the complex was not performed. However the solution-phase ^{31}P NMR spectrum of the complex showed three phosphorus environments, as expected for the simultaneous κ^1-P,κ^3-P,O,P-binding of the ligand, of which one had a chemical shift value close to that of uncoordinated phosphine. The tridentate nature of the DBFphos ligand was unambiguously confirmed during the synthesis and subsequent X-ray analysis of *mer*-$Ru(Cl)_2(PR_3)(\kappa^3$-P,O,P-DBFphos) (R = Ph and *p*-tol), which showed a wide bite angle (155.2(1)°) and close Ru—O distance of 2.101(2) Å for the R = Ph derivative.

6. DPEphos-type ligands

DPEphos was initially synthesised by van Leeuwen and co-workers in 1995 for use as a κ^2-P,P-bidentate ligand [12]. Its natural bite angle of 102.2° was calculated to be lower than that of Xantphos-type ligands. Many reports have also suggested that due to the lack of a CMe_2 linker in its backbone, the DPEphos ligand is more flexible than its Xantphos-type counterparts.

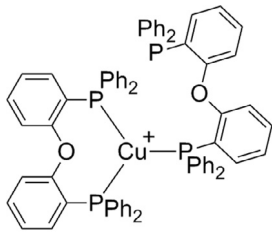

77

Fig. 6. Structure of $[Cu(DPEphos)_2]^+$ showing the tricoordinate Cu(I) centre. BF_4 anion omitted for clarity.

The complex $[Cu(DPEphos)_2][BF_4]$ (**77**), synthesised by Venkateswaran et al. [71], revealed one ^{31}P environment for the four phosphine groups at room temperature. However at −50 °C the signal broadened, indicating fluxional behaviour in solution. In fact, the solid-state structure of the complex showed a tricoordinate Cu centre, with three short Cu—P bond lengths of 2.2686(8) Å, 2.2719(8) Å and 2.2782(9) Å, and one much longer Cu—P distance demonstrating an unbound phosphine ligand (3.9576(9) Å) (Fig. 6), i.e. DPEphos behaves as both a κ^2-P,P and κ^1-P-ligand in the same molecule. It was postulated that the fourth phosphine ligand was unable to establish a Cu—P bond due to the relative bulkiness of the ligand in comparison to the analogous complex of the diphenylphosphinoethane (dppe) ligand, which does form a tetracoordinated solid-state structure with copper. It was proposed that the solution-phase fluxional behaviour demonstrated by the DPEphos ligand involved the coordination/decoordination of each phosphine arm. κ^1-P-coordination of the DPEphos ligand was also observed in the formation of bimetallic gold complexes, where the two phosphines on the same ligand each bond to different gold atoms (e.g., complex **67**, Scheme 21) [63,64].

In a report by Balakrishna and co-workers, ruthenium complexes of DPEphos, incorporating *cis*-κ^2-P,P, *fac*-κ^3-P,O,P and *mer*-κ^3-P,O,P coordination were crystallographically characterised (Scheme 24) [72]. For example, the synthesis of *fac*-$Ru(Cl)_2(S(O)Me_2)(\kappa^3$-P,O,P-DPEphos) (**78**) allowed measurement of the Ru—O bond length of 2.209(2) Å and narrow P—Ru—P angle of 99.16(3)°. Addition of PPh_3 to this *fac*-κ^3-P,O,P-complex resulted in the formation of *mer*-$[Ru(Cl)_2(PPh_3)(\kappa^3$-P,O,P-DPEphos)] (**79**) (Ru—O = 2.235(3) Å, P—Ru—P = 158.53(4)°) as confirmed by widening of the P—Ru—P angle but retention of the short metal–oxygen bond. The variable coordination-mode ability of the DPEphos ligand was observed on addition of two equivalents of pyridine to complex **78**, yielding *trans*,*cis*-$Ru(Cl)_2(py)_2(\kappa^2$-P,P-DPEphos) (**80**). The authors proposed that the first step of this reaction was through dissociation of the DPEphos ether linkage to reveal a vacant site to which the first pyridine molecule could bind (Scheme 24). The lack of Ru—O bond in the *cis*-κ^2-P,P-complex was shown by a distance of 3.287(2) Å present between the two atoms.

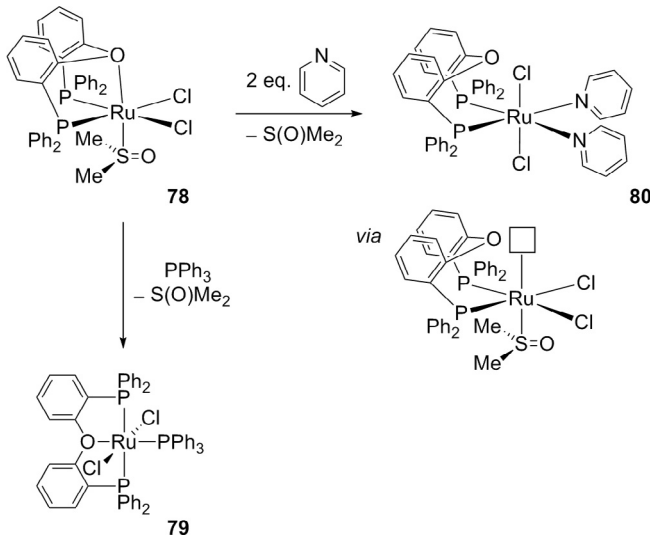

Scheme 24. Ligand substitution reactions of complex **78** which showed *fac*-κ^3-P,O,P, *mer*-κ^3-P,O,P and *cis*-κ^2-P,P-binding of the ligand.

The Weller group reported that on placing *fac*-$[Rh\{PCyp_2(\eta^2$-$C_5H_7)\}(\kappa^3$-P,O,P-DPEphos$)][BAr^F_4]$ (Cyp = cyclopentyl) (**81**) under an H_2 atmosphere, the bound alkene was hydrogenated and at room temperature the major species formed was *fac*-$[Rh(H)_2(PCyp_3)(\kappa^3$-P,O,P-DPEphos$)][BAr^F_4]$ (**82**) (Scheme 25), which was characterised by single crystal X-ray diffraction (Rh—O = 2.308(2) Å, P—Rh—P = 99.20(3)°) [73]. At −50 °C under H_2 this complex was in equilibrium with the dihydrogen dihydride complex *cis*-$[Rh(\eta^2$-$H_2)(H)_2(PCyp_3)(\kappa^2$-P,P-DPEphos$)][BAr^F_4]$ (**83**). In order for this equilibrium to occur, the central ether linkage of the DPEphos ligand must dissociate from the metal to allow coordination of a dihydrogen molecule, hence acting in a hemilabile manner (Scheme 25). Addition of MeCN to this equilibrium mixture at room temperature displaced the η^2-H_2 ligand, giving *cis*-$[Rh(NCMe)(H)_2(PCyp_3)(\kappa^2$-P,P-DPEphos$)][BAr^F_4]$ (**84**), confirming the likely structure of the dihydride dihydrogen complex formed at low temperatures. H_2 loss from **82**/**83** occurred through reductive elimination to form Rh(I) *mer*-$[Rh(PCyp_3)(\kappa^3$-P,O,P-DPEphos$)][BAr^F_4]$ (**85**). In comparison, the analogous study using the Xantphos-Ph ligand showed that the dihydrogen adduct *cis*-$[Rh(\eta^2$-$H_2)(H)_2(PCyp_3)(\kappa^2$-P,P-Xantphos-Ph$)][BAr^F_4]$ was not formed in equilibrium with *fac*-$[Rh(H)_2(PCyp_3)(\kappa^3$-P,O,P-Xantphos-Ph)] (**86**), but instead *fac*–*mer* isomerisation occurred from which the corresponding *mer*-isomer, *mer*-$[Rh(H)_2(PCyp_3)(\kappa^3$-P,O,P-Xantphos-Ph)] (**87**), could be observed (Scheme 25) – indicating that the Rh—O bond in the Xantphos-Ph complex were more persistent in the analogous DPEphos complexes and must outcompete H_2 bond-

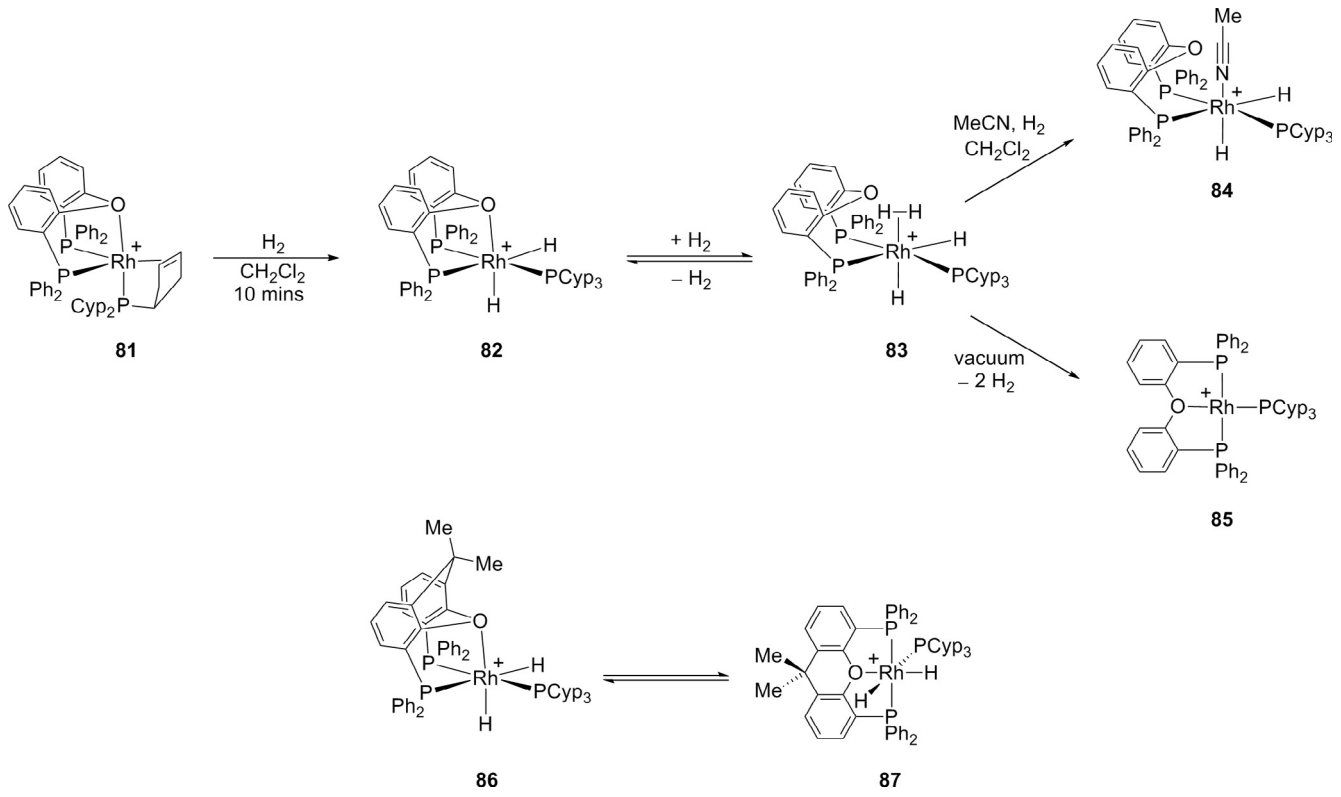

Scheme 25. Variable binding modes of DPEphos and difference in ability for the DPEphos ligand to dissociate the ether linker during the coordination of H_2 compared to that of Xantphos-Ph. BAr^F_4 anions omitted for clarity.

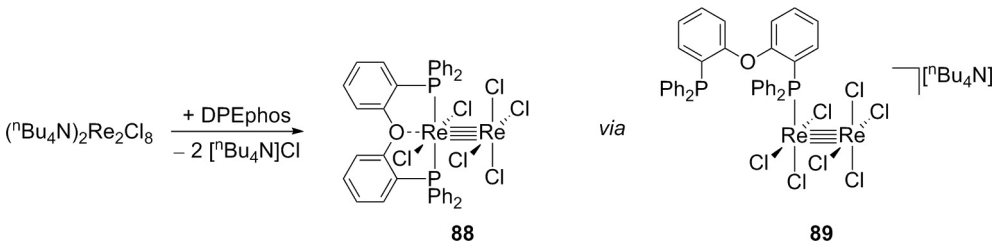

Scheme 26. The postulated formation of complex **88** via the κ^1-P-DPEphos intermediate **89**.

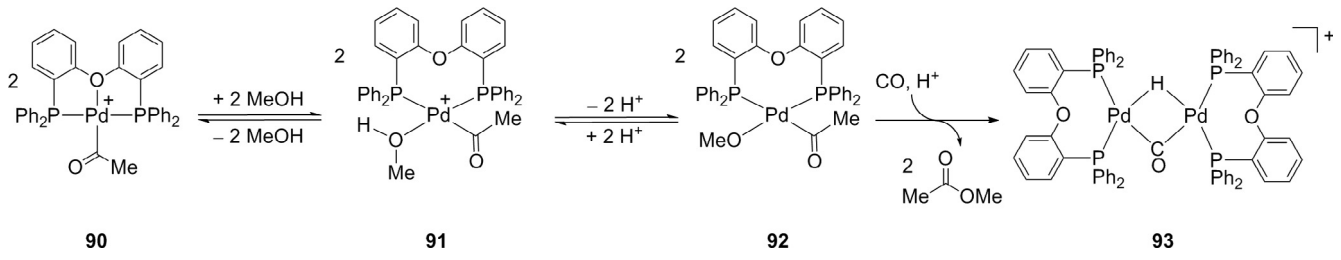

Scheme 27. Proposed mechanism of methanolysis by *mer*-$[Pd(C(O)CH_3)(\kappa^3\text{-P,O,P-DPEphos})]^+$ to form methylpropanoate. OTf anion omitted for clarity.

ing. The MeCN adduct, analogous to **84**, could be formed, though. Equilibrium studies showed that the *fac*-isomer **86** was slightly favoured over the *mer* (**87**), due to entropic factors. The Xantphos isomers **86** and **87** also lost H_2 to form the corresponding *mer*-Rh (I) complex, *mer*-$[Rh(PCyp_3)(\kappa^3\text{-P,O,P-Xantphos})][BAr^F_4]$, analogous to complex **85**, and this was observed to be faster than for the DPEphos variants.

As for Xantphos-Ph complexes described previously, the reactivity of DPEphos complexes may also require the dissociation of one of the phosphine arms, to form intermediates that contain a κ^1-P-DPEphos binding mode. Such behaviour was reported by Walton and co-workers, in which the formation of *mer*-$Re_2(Cl)_6(\kappa^3\text{-P,O,P-DPEphos})$ (**88**) from $(^nBu_4N)_2Re_2Cl_8$ was proposed to proceed through a $[Re_2(Cl)_7(\kappa^1\text{-P-DPEphos})][^nBu_4N]$ intermediate (**89**), as shown in Scheme 26 [69]. The final complex **88** was suggested to contain a *mer*-κ^3-P,O,P-bound DPEPhos ligand with a weak Re—O interaction; however the crystal structure of the complex could not be obtained.

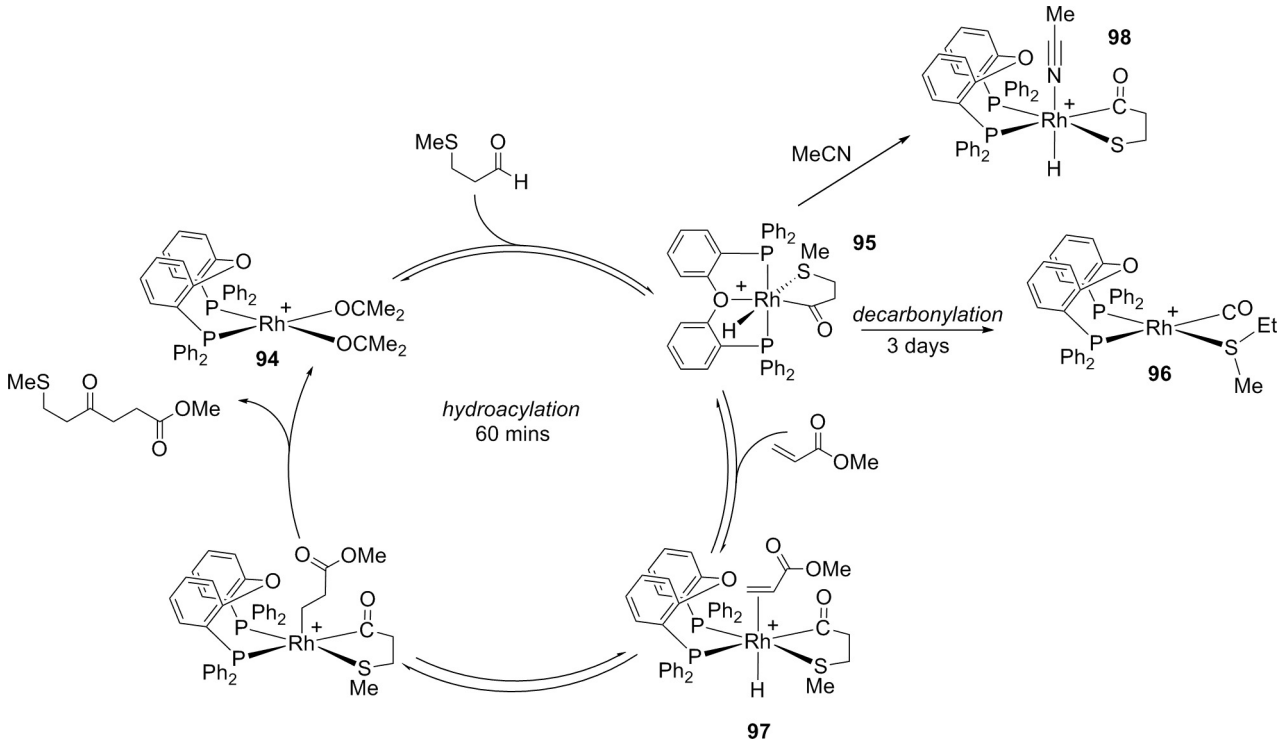

Scheme 28. Proposed catalytic cycle for the hydroacylation of alkenes using the {Rh(DPEphos)} fragment. $CB_{11}H_6Cl_6$ anion omitted for clarity.

The importance of the *cis* or *trans*-bound nature of the DPEphos ligand was explored in 2003 by van Leeuwen and co-workers, in their study of alcoholysis of acylpalladium complexes to form esters [74]. *mer*-[Pd(C(O)CH_3)(κ^3-P,O,P-DPEphos)][OTf] (**90**) was shown to react with methanol to form methylpropanoate, in doing so dissociating the DPEphos ether linkage to allow coordination of methanol at the metal centre, which formed a *cis*-[Rh(C(O)CH_3)(MeOH)(κ^2-P,P-DPEphos)][CF_3SO_3] (**91**) intermediate which could be deprotonated to form an intermediate such as **92**. Subsequent reductive elimination of methylpropanoate from **92**, under a CO atmosphere, afforded the bimetallic rhodium complex (**93**) (Scheme 27), presumably *via* a Pd(0) intermediate that undergoes protonation and coordination of CO. DPEphos was postulated to be flexible enough to allow for both *mer*-κ^3-P,O,P and *cis*-κ^2-P,P complexes to form over the course of the reaction, as the association of methanol was rate determining, and therefore the switch of ligand binding mode between complexes **90** and **91** was important for the overall rate. $\Delta G^{\ddagger}$ for this transformation was estimated to be +83 kJ mol^{-1}, whereas the analogous system involving the Xantphos-Ph ligand had a significantly higher barrier, $\Delta G^{\ddagger}$ = +92 kJ mol^{-1}. This increased barrier suggests that oxygen dissociation and ligand reorganisation of the Xantphos-Ph ligand was less favourable than for DPEphos.

The hemilabile nature of DPEphos was exploited by Moxham et al. in studies centred on the hydroacylation reaction of alkenes using aldehydes by the *in situ* formed precatalyst *cis*-[Rh($OCMe_2$)$_2$(κ^2-P,P-DPEphos)][$CB_{11}H_6Cl_6$] (**94**, Scheme 28) [28]. Hydroacylation involves a C—H activation of an aldehyde at a Rh(I) centre, followed by insertion of an olefin or alkyne and reductive elimination of a ketone product. There are therefore oxidation state changes and a requirement for formation of latent coordination sites during catalysis. A problem that persists during catalysis is the reductive decarbonylation from a low-coordinate acyl hydride intermediate that arises from oxidative addition of the aldehyde, which results in catalyst deactivation. The DPEphos ligand was shown to be able to stabilise the acyl hydride intermediate formed by aldehyde addition to **94** by coordination of the ether linker, forming *mer*-[Rh(H)($MeSCH_2CH_2CO$)(κ^3-P,O,P-DPEphos)][$CB_{11}H_6Cl_6$] (**95**) which was characterised *in situ* using NMR spectroscopy. As reductive decarbonylation of this species to form **96** was much slower than with other, non-hemilabile ligands, such as dppe, this allowed for more challenging substrates to be tackled in hydroacylation catalysis. For productive hydroacylation to occur, however, dissociation of the bound oxygen is required prior to binding of alkene, which was expected to form *cis*-[Rh(H)(η^2-H_2C=CHCOOMe)($MeSCH_2CH_2CO$)(κ^2-P,P-DPEphos)][$CB_{11}H_6Cl_6$] (**97**). To support this, acetonitrile was added to the acyl hydride intermediate as a proxy for alkene, and the resultant solid-state structure showed *cis*-[Rh(H)(NCMe)($MeSCH_2CH_2CO$)(κ^2-P,P-DPEphos)][$CB_{11}H_6Cl_6$] (**98**), in which the phosphine ligands were bound *cis* (P—Rh—P = 100.37 (3)°) and the oxygen atom was no longer coordinated [Rh···O = 4.271(1) Å]. The overall proposed catalytic cycle for this transformation is detailed in Scheme 28 and shows the importance of the ability for the DPEphos ether group to bind to the metal centre to stabilise intermediates, as well as dissociate from rhodium in order to allow further reactivity to occur. Notably, the use of the ligands POP-Ph (Scheme 5) and Xantphos-Ph in place of DPEphos did not lead to productive hydroacylation catalysis [27], as the central oxygen atoms were too strongly bound in the *mer*-κ^3-P,O,P geometry (similar to complex **95**) to allow for alkene complexation.

Continuing the theme of hydroacylation, the Weller group again utilised the {Rh(κ^2-P,P-DPEphos)}$^+$ precatalyst **94** for the hydroacylation of alkynes to form α,β-unsaturated ketones [75]. As shown in Scheme 29 the stabilisation of *fac*-κ^3-P,O,P and *cis*-κ^2-P,P intermediate complexes demonstrated the importance of the hemilability of the ligand during such transformations. In particular, the isolation of the branched alkenyl intermediate (complex **99**) which preceded turnover-limiting reductive elimination enabled the mechanism of this reaction to be studied in detail. The *fac*-κ^3-P,O,P binding of the ligand in this complex was demonstrated by the solid-state structure as confirmed by single crystal X-ray diffraction studies (P—Rh—P = 95.41(2)°,

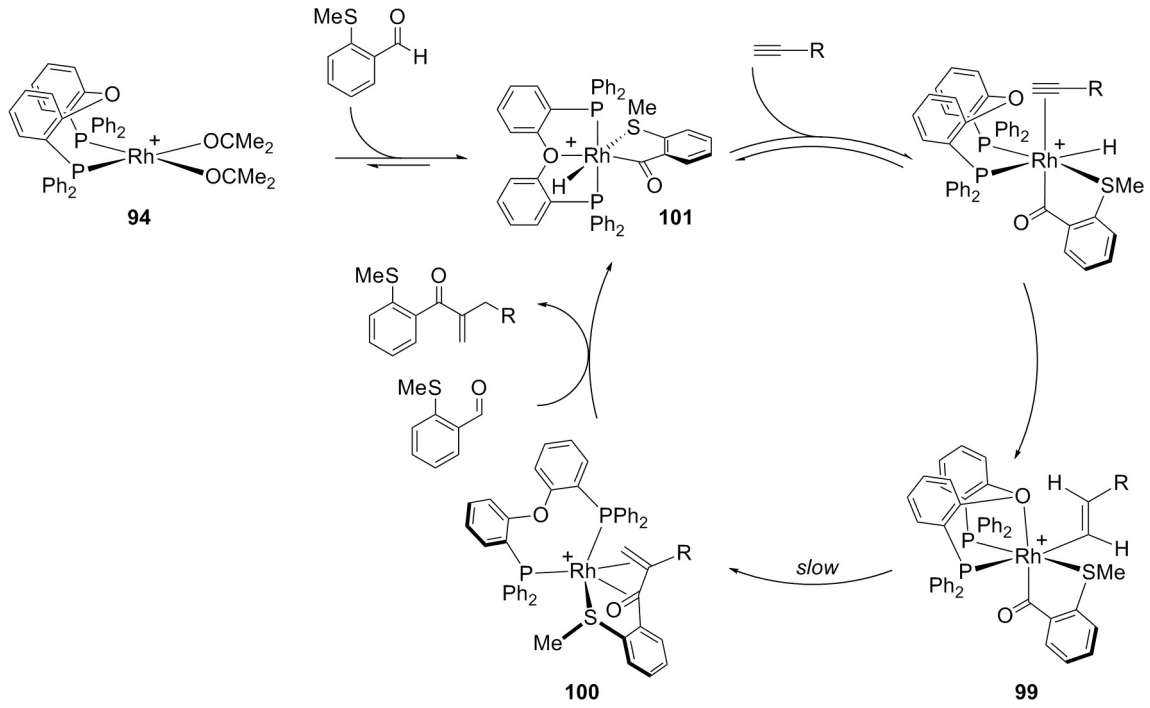

Scheme 29. Proposed catalytic cycle for the hydroacylation of alkynes to form the branched alkenyl product using the {Rh(DPEphos)} fragment. $CB_{11}H_{12}$ anion omitted for clarity.

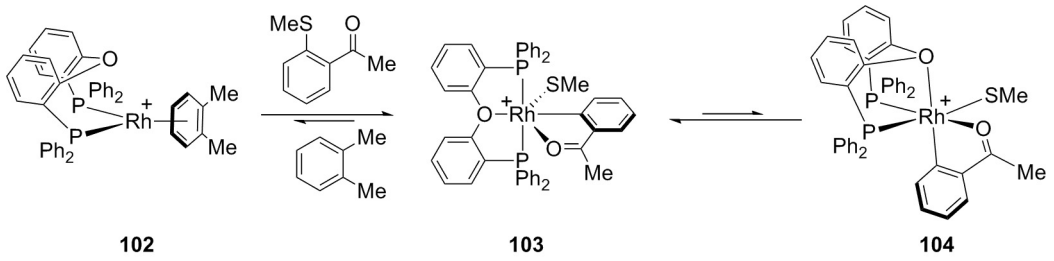

Scheme 30. *fac–mer* isomerisation of the catalyst resting state during the carbothiolation of alkynes using a $\{Rh(DPEphos)\}^+$ fragment. BAr^F_4 anions omitted for clarity.

Rh—O = 2.3458(17) Å). The α,β-unsaturated ketone product was found to bind to the metal centre after a slow reductive elimination event from this alkenyl complex, which yielded a 5-coordinate complex (**100**) – where the crystal structure showed a *cis*-κ^2-P,P binding mode of the DPEphos ligand, indicated by the P—Rh—P bite angle of 97.87(5)° and long Rh···O distance (3.395(5) Å). The ketone product was released from the metal centre with oxidative addition of the starting aldehyde and coordination of the DPEphos ether group, and reformed the *mer*-κ^3-P,O,P acyl hydride species (**101**).

Another example of catalysis in which the DPEphos was used with success, and the flexible nature of the ligand shown, was in alkyne carbothiolation [31]. The Rh(I) κ^2-P,P-DPEphos precatalyst (**102**) oxidatively added an aryl methyl sulphide to form a *mer*-κ^3-P,O,P-DPEphos complex (**103**), which was in equilibrium with its analogous *fac*-κ^3-P,O,P complex (**104**) (Scheme 30). This equilibrium was proposed to operate through a 5-coordinate intermediate where the DPEphos oxygen dissociated from the metal in order to access a conformationally flexible species required for *fac–mer* isomerisation. Similar behaviour was noted with the Xantphos-Ph ligand in which it was demonstrated that the *fac*-κ^3-P,O,P-Xantphos-Ph catalyst was a more active catalyst than the *mer* (Scheme 17) [30].

κ^2-P,P to κ^1-P-coordination of the DPEphos ligand was proposed to be important in a study by Ohshima et al. in the platinum-catalysed amination of allylic alcohols which utilised an *in situ* formed catalyst from $Pt(COD)Cl_2$/DPEphos [76]. It was found that a 1:1 ratio of Pt:DPEphos gave rise to the formation of a black precipitate during catalysis – a result of decomposition of the active Pd(0) species. To combat this, two equivalents of DPEphos with respect to the metal were employed in an attempt to stabilise the active species by formation of $Pt(\kappa^2$-P,P-DPEphos$)_2$. This coordinatively saturated complex was an active precatalyst, and it was speculated that complete dissociation of one of the DPEphos ligands, or alternatively decoordination of just one of the DPEphos phosphine arms to form a coordinatively unsaturated platinum metal centre with a κ^1-P-DPEphos ligand, allowed a coordinatively unsaturated, active Pt(0) catalyst to form. This method of stabilising the active species towards decomposition was also attempted using the Xantphos-Ph ligand, however the corresponding $Pt(\kappa^2$-P,P-Xantphos-Ph$)_2$ complex showed limited solubility in toluene, the reaction solvent of choice.

A very recent study carried out by Goldberg and co-workers [77], investigated the use of rhodium complexes containing the DPEphos ligand for the reductive elimination of products with C

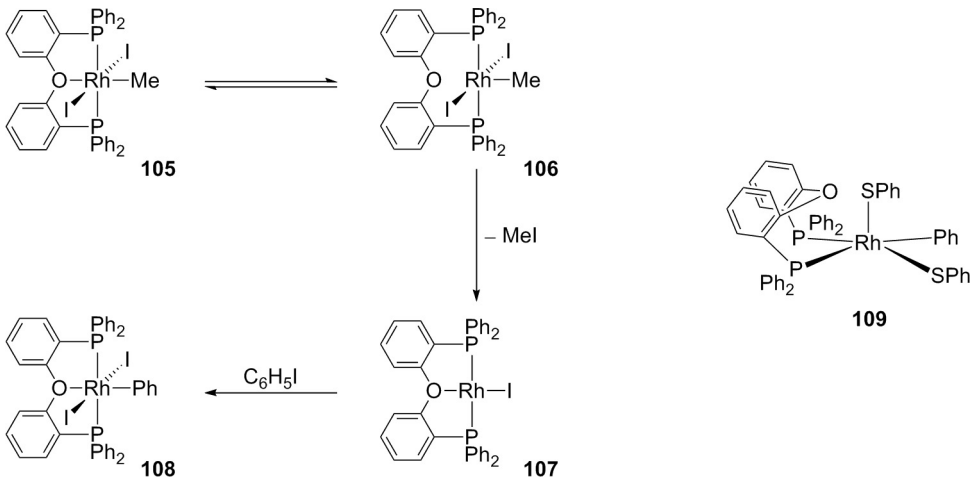

Scheme 31. One of the nucleophilic pathways postulated for reductive elimination of compounds with C(sp^3)—I bonds. The proposed structure of the end organometallic product of C(sp^3)—S bond formation is shown (**109**).

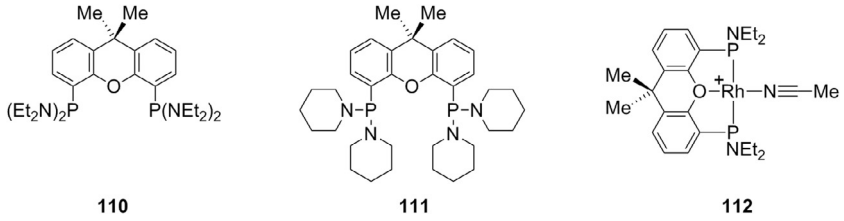

Fig. 7. Aminophosphine Xantphos ligands used for the intramolecular hydroamination of aminoalkenes. The precatalyst containing ligand **110**, complex **112**, could be crystallographically characterised. BF_4 anion omitted for clarity.

(sp^3)—X bonds (X = N, S, I). The elimination of MeI from *mer*-Rh(Me)$(I)_2(\kappa^3$-P,O,P-DPEphos) (**105**) was found to occur *via* two competing pathways which both involved S_N2 attack of the iodide on the methyl group of either a neutral or cationic species. The mechanism detailed in Scheme 31 was suggested to involve initial decoordination of the DPEphos ether linkage from the metal in complex **105** to form complex **106**, *trans*-Rh(Me)$(I)_2(\kappa^2$-P,P-DPEphos) that then underwent attack by iodide, and subsequent elimination of MeI. The hemilability of the DPEphos was suggested to increase the electrophilic nature of the methyl group and encourage nucleophilic attack of the iodide to eventually form the final product *mer*-Rh(I)$(\kappa^3$-P,O,P-DPEphos) (**107**) with loss of MeI. Reaction with the solvent, iodobenzene, formed *mer*-Rh(Ph)$(I)_2(\kappa^3$-P,O,P-DPEphos) (**108**). Addition of excess sodium thiophenolate to complex **105** gave the corresponding MeSPh product, square pyramidal *cis*-Rh(Ph)$(SPh)_2(\kappa^2$-P,P-DPEphos) (**109**).

A DFT study on alkene hydroamination reactions catalysed by the $\{Rh(DPEphos)\}^+$ catalyst [78] was published by Couce-Rios et al. in 2016 [79]. In this, structural isomers (κ^2-P,P-DPEphos versus κ^3-P,O,P-DPEphos) of proposed intermediates along the calculated reaction pathway were studied. Interestingly, the structures for which DPEphos occupied κ^3-P,O,P coordination sites were more than 6 kcal mol^{-1} higher in energy than their κ^2-P,P-DPEphos analogues.

7. Miscellaneous ligands

7.1. Xantphos-type ligands containing aminophosphine groups

Xantphos-type ligands containing aminophosphine groups have been developed by van Leeuwen [80] and Hartwig (e.g., compounds **110** and **111**, Fig. 7) [81]. In particular, Hartwig reported their use in rhodium-catalysed intramolecular hydroamination of aminoalkenes, which proved to be advantageous compared to the same reactions with the more ubiquitous Xantphos-Ph or Xantphos-Cy analogues. The Xantphos-NEt_2 ligands (e.g., **110**) led to the best conversions, and also showed the greatest selectivity for hydroamination over oxidative amination, attributed to the *mer*-κ^3-P,O,P binding mode of the ligand to the rhodium centre, which may inhibit any possible *beta*-hydride-elimination (Scheme 4) and therefore prevented formation of unwanted oxidative amination products. The κ^3-P,O,P-tridentate binding mode of the Xantphos-NEt_2 ligand was confirmed by an X-ray diffraction study of the precatalyst, *mer*-[Rh(NCMe)(κ^3-P,O,P-Xantphos-NEt_2)][BF_4] (**112**, Fig. 7), and showed a short Rh—O bond of 2.129 (8) Å and a wide P—Rh—P angle of 168.0(1)°, whilst the proposed catalytic cycle retained κ^3-P,O,P-coordination of the ligand in the formation of intermediates. The activity of the aminophosphine ligand **110** in hydroamination catalysis was around twice that of the Xantphos-Cy and Xantphos-Ph ligands, therefore the electronic and steric effects of the ligands were compared. The complexes {Rh(CO)(Xantphos-NEt_2)}$^+$ and {Rh(CO)(Xantphos-Cy)}$^+$ were synthesised, and their ν_{CO} values were found to be 1993.3 cm^{-1} and 1992.7 cm^{-1} respectively, indicating that both the amino and alkyl Xantphos ligands have similar electron-donating effects to the metal centre. In addition, a Xantphos-type ligand containing piperidinyl groups (**111**) was proposed to be isosteric to Xantphos-Cy, but showed increased reactivity similar to that of Xantphos-NEt_2, therefore steric factors were also speculated to not be of importance. The authors suggested that the effect of the substituents cannot be attributed to steric or electronic demands, though other reasoning was not explored. Aminophosphine Xantphos-NR_2 ligands such as **110** and **111** have not yet been explored for their hemilabile capabilities.

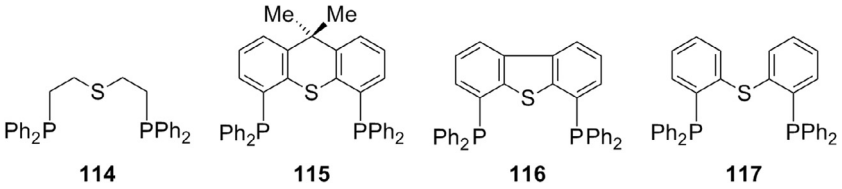

Fig. 8. Examples of PSP-type ligands known in the current literature.

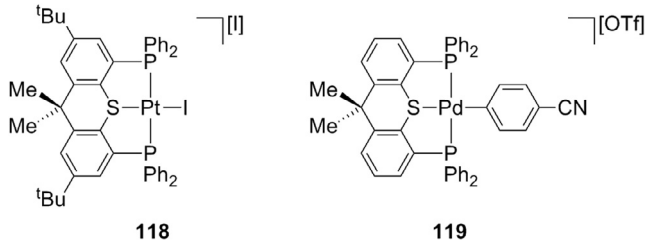

Fig. 9. Transition metal complexes synthesised which are proposed to contain Thioxantphos-type ligands coordinated to the metal centre in a *mer*-κ^3-P,S,P fashion.

7.2. PSP-type ligands

Whilst the sulphur-containing analogues of POP (bis(2-diphenylphosphinoethyl)sulphide, "PSP") Xantphos (4,5-bis(diphenylphosphino)-9,9,-dimethylthioxanthene, "Thioxantphos"), DBFphos (4,6-bis(diphenylphosphino)dibenzothiophene) and DPEphos (bis[(2-diphenylphosphino)phenyl] thioether) – depicted in Fig. 8 as ligands **114**, **115**, **116** and **117** respectively – have been synthesised, transition metal complexes of these ligands are relatively rare compared to their oxygen counterparts. Thus far, no complexes containing 4,5-bis(diphenylphosphino)dibenzothiophene (**116**) have been structurally characterised, however the crystal structure of the ligand was reported by Haenel and co-workers in 1993 [82].

Examples of transition metal complexes containing the PSP ligand (**114**) have been structurally characterised, where the ligand can bind in both *cis*-κ^2-P,P [83] and *mer*-κ^3-P,S,P geometries [84–87]. Isomerisation between *fac*-κ^3-P,S,P and *mer*-κ^3-P,S,P complexes of **114** has also been reported [87]. Whilst there are currently no solid-state structures of Thioxantphos complexes reported in the literature, a 2008 study by Emslie and co-workers utilised the Thioxantphos derivative, 2,7-di-*tert*-butyl-4,5-bis(phenylphosphino)-9,9-dimethylthioxanthene, to obtain the platinum complex **118** (Fig. 9) in which the ligand was bound in a *mer*-κ^3-P,S,P fashion showing a short Pt—S bond (2.252(2) Å) and a wide P—Pt—P angle (165.38(6)°) [88]. In 2002, Zuideveld et al. synthesised transition metal complexes containing the {Pd(Thioxantphos)} fragment [41], e.g., complex **119** (Fig. 9). These complexes were proposed to be ionic through molar conductivity studies, therefore indicating *mer*-κ^3-P,S,P-Thioxantphos coordination. Interestingly, complex **119** was shown to be inactive in the amination of aryl triflates (see Scheme 14 for analogous Xantphos reactivity), postulated to be due to strong coordination of the soft sulphur atom to the palladium metal centre which is not readily dissociated to allow for onward reactivity [48].

The proposed strong binding of sulphur to transition metals was also demonstrated in work involving ligands based upon bis[(2-diphenylphosphino)phenyl]thioether (**117**). Weller and co-workers showed that [Rh(nbd)(**117**)][$CbCl_6$] (nbd = 2,5-norbornadiene, $CbCl_6$ = *closo*-$CB_{11}H_6Cl_6$) (complex **120**, Scheme 32) was in fact a κ^3-P,S,P structure by an X-ray diffraction study (Rh—S = 2.2955(5) Å, P—Rh—P = 103.38(2)°), whilst the DPEphos analogue existed as *cis*-{Rh(nbd)(κ^2-P,P-DPEphos)}$^+$ [29]. In addition, complex **120** was inactive in hydroacylation catalysis, unlike its DPEphos counterpart [28,29], again predicted to be due to the strong binding of sulphur with the metal centre. Variable coordination modes of ligands based upon **117** were shown by Morohashi et al. in which a derivative of **117**, (bis[(2-diphenylphosphino-5-*tert*-butyl)phenyl]thioether) formed both *cis*-κ^2-P,P and *mer*-κ^3-P,S,P complexes of platinum (complexes **121** and **122** respectively, Scheme 32) [89]. The geometry of the ligand in **121** was shown to be *cis*-κ^2-P,S,P by its solid-state structure which contained a narrow P—Pd—P bond angle of 96.32(3)° and long Pd—S bond measured to be 2.9867(8) Å. On addition of AgOTf to complex **121** (Scheme 32), abstraction of one of the chloride ligands yielded the corresponding *mer*-κ^3-P,S,P-bound complex **122**, which was additionally confirmed by X-ray crystallography (Rh—S = 2.2685(30) Å, P—Rh—P = 167.52(10)°). This reactivity showed that this type of ligand was capable of altering its denticity to a metal centre enforced by the electronic constraints on the metal, thus behaving in both *cis*-κ^2-P,P and *mer*-κ^3-P,S,P coordination modes.

8. Concluding remarks

This review has explored examples of hemilabile-type behaviour and flexible coordination modes of POP-type ligands in transition metal complexes. The subtle interplay between sterics (imposed by the appended phosphine groups) and ligand flexibility or bite angle (stemming from the nature of the ligand backbone), plays an important role in determining the κ^1-P, κ^2-P,P or κ^3-P,O,P-coordination mode of the POP-ligand with the metal. In particular, the ether linker has the capacity to occupy vacant sites in low-coordinate complexes, but may remain easy enough to dissociate

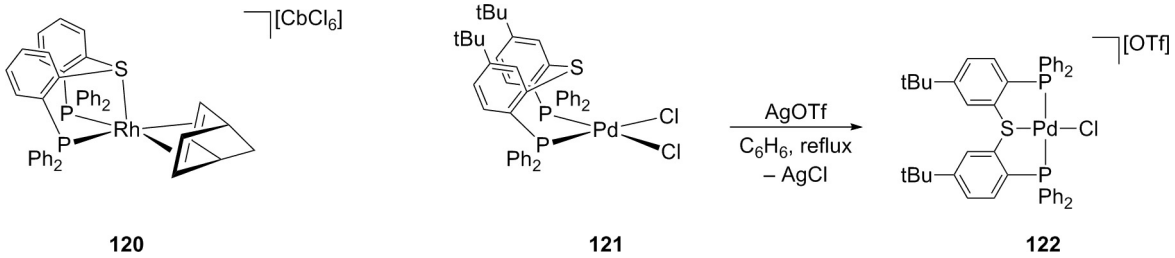

Scheme 32. Left: Structure of complex **120** which has been crystallographically characterised to show the *fac*-κ^3-P,S,P coordination of the PSP-type ligand. Right: Variable coordination modes of a derivative of ligand **117** (Fig. 8), both the *cis*-κ^2-P,P in **121** and *mer*-κ^3-P,S,P coordination in **122** was shown by X-ray diffraction studies.

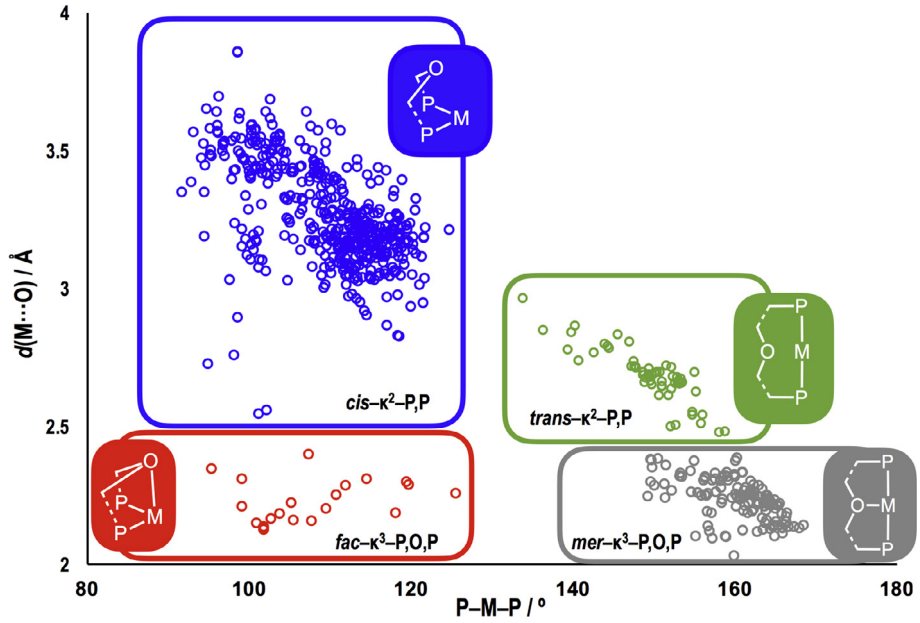

Fig. 10. Plot of M—O distance (Å) versus P—M—P bite angle (°) in crystallographically characterised transition metal complexes containing POP-type ligands.

from the metal centre to allow the coordination of incoming substrates. Perhaps surprisingly, but persuasively, calculations have also demonstrated that the phosphine groups may have the capacity for such hemilabile behaviour as well.

Throughout the current literature and discussed in this review, the M—O bond distance and P—M—P bond angle of crystallographically characterised complexes containing POP-type ligands have been helpful in determining the coordination geometry of the ligand. Building on the graphical representation of M—O bond distance versus P—M—P bond angle for Xantphos-Ph complexes reported by Haynes and co-workers (Fig. 3) [33], we now construct the analogous graph for all complexes contained in Cambridge Structural Database (CSD) containing a POP-type ligand (Fig. 10) [90–92]. The clustering of data in Fig. 10 allows for demarcation of the four possible coordination geometries of POP-type ligands in transition metal complexes, although data which sit close to a boundary should be more closely interrogated to determine the precise bonding mode. In general, complexes with long M—O distances and small bite angles (M—O > 2.5 Å, P—M—P < 125°) are considered to be *cis*-κ^2-P,P-POP-type complexes with no formal metal–oxygen bond and lie at the top left of the plot. *trans*-κ^2-P,P-POP-type complexes where the bite angle is large, but the M—O distance remains long, are situated to the top right of the plot (M—O > 2.4 Å, P—M—P > 130°). There may be an inherent, at best weak, metal–oxygen interaction present in some of these complexes due to the close proximity of the metal and oxygen atoms caused by the *trans*-spanning nature of the POP-type ligand. Complexes occupying the bottom right of the graph are *mer*-κ^3-P,O,P-complexes, in which M—O distances are shorter and the phosphine ligands are situated *trans* (M—O < 2.4 Å, P—M—P > 145°). This subset of ligand geometry can be considered to be pincer-like. The final set of coordination complexes are found at the bottom left of the figure, containing complexes with both short M—O distances and narrow bite angles (M—O < 2.4 Å, P—M—P < 130°), which are examples of *fac*-κ^3-P,O,P structures, where the phosphine ligands lie *cis* to one another, and the ether linker lies in the apical position of the complex, and *cis* to both phosphines.

The ability of POP-type ligands to adapt their denticity in a variety of ways to respond to the requirements of the metal centre shows their versatility for the fine-tuning of reactivity of their associated transition metal complexes. Given the body of work that already exists, there is no doubt that the flexible coordination modes and hemilability of POP-type ligands will lead to their increased use in the synthesis of tailor-made homogeneous catalysts, which often – of course – require variable and accessible coordination geometries throughout the catalytic cycle.

Acknowledgements

We thank the EPSRC (EP/M024210) and the University of Oxford for support.

Appendix A. Supplementary data

Supplementary data associated with this article can be found, in the online version, at http://dx.doi.org/10.1016/j.ccr.2017.08.004.

References

[1] J.F. Hartwig, Organotransition Metal Chemistry, University Science Books, Sausalito, USA, 2010.
[2] P.W.N.M. van Leeuwen, J.C. Chadwick, Homogeneous Catalysis, Wiley-VCH, Wennheim, 2011.
[3] Z. Freixa, P.W.N.M. van Leeuwen, Dalton Trans. (2003) 1890–1901.
[4] M.-N. Birkholz, Z. Freixa, P.W.N.M. van Leeuwen, Chem. Soc. Rev. 38 (2009) 1099–1118.
[5] D. Morales-Morales, C. Jensen, The Chemistry of Pincer Compounds, Elsevier, Amsterdam, 2007.
[6] G. van Koten, Top. Organomet. Chem. 40 (2013) 1–20.
[7] C. Gunanathan, D. Milstein, Acc. Chem. Res. 44 (2011) 588–602.
[8] J. Choi, A.H.R. MacArthur, M. Brookhart, A.S. Goldman, Chem. Rev. 111 (2011) 1761–1779.
[9] N. Selander, K.J. Szabó, Chem. Rev. 111 (2011) 2048–2076.
[10] C. Gunanathan, D. Milstein, Chem. Rev. 114 (2014) 12024–12087.
[11] H.A. Younus, N. Ahmad, W. Su, F. Verpoort, Coord. Chem. Rev. 276 (2014) 112–152.
[12] M. Kranenburg, Y.E.M. van der Burgt, P.C.J. Kamer, P.W.N.M. van Leeuwen, K. Goubitz, J. Fraanje, Organometallics 14 (1995) 3081–3089.
[13] J.C. Jeffrey, T.B. Rauchfuss, Inorg. Chem. 18 (1979) 2658–2666.
[14] A. Bader, E. Lindner, Coord. Chem. Rev. 108 (1991) 27–110.
[15] C.S. Slone, D.A. Weinberger, C.A. Mirkin, Prog. Inorg. Chem. 48 (1999) 233–350.
[16] P. Braunstein, F. Naud, Angew. Chem. Int. Ed. 40 (2001) 680–699.
[17] M. Bassetti, Eur. J. Inorg. Chem. (2006) 4473–4482.
[18] C.G. Oliveri, P.A. Ulmann, M.J. Wiester, C.A. Mirkin, Acc. Chem. Res. 41 (2008) 1618–1629.
[19] Z. Weng, S. Teo, T.S.A. Hor, Acc. Chem. Res. 40 (2007) 676–684.

[20] N.W. Alcock, J.M. Brown, J.C. Jeffery, J. Chem. Soc., Chem. Commun. (1974) 829–830.
[21] N.W. Alcock, J.M. Brown, J.C. Jeffery, J. Chem. Soc., Dalton Trans. (1976) 583–588.
[22] P.T. Greene, L. Sacconi, J. Chem. Soc. A (1970) 866–872.
[23] Q. Major, A.J. Lough, D.G. Gusev, Organometallics 24 (2005) 2492–2501.
[24] C. Bolzati, A. Boschi, A. Duatti, S. Prakash, L. Uccelli, F. Refosco, F. Tisato, G. Bandoli, J. Am. Chem. Soc. 122 (2000) 4510–4511.
[25] C. Bolzati, A. Boschi, L. Uccelli, F. Tisato, F. Refosco, A. Cagnolini, A. Duatti, S. Prakash, G. Bandoli, A. Vittadini, J. Am. Chem. Soc. 124 (2002) 11468–11479.
[26] A. Buhling, P.C.J. Kamer, P.W.N.M. van Leeuwen, J.W. Elgersma, K. Goubitz, J. Fraanje, Organometallics 16 (1997) 3027–3037.
[27] R.J. Pawley, G.L. Moxham, R. Dallanegra, A.B. Chaplin, S.K. Brayshaw, A.S. Weller, M.C. Willis, Organometallics 29 (2010) 1717–1728.
[28] G.L. Moxham, H.E. Randell-Sly, S.K. Brayshaw, R.L. Woodward, A.S. Weller, M.C. Willis, Angew. Chem. Int. Ed. 45 (2006) 7618–7622.
[29] G.L. Moxham, H. Randell-Sly, S.K. Brayshaw, A.S. Weller, M.C. Willis, Chem. Eur. J. 14 (2008) 8383–8397.
[30] P. Ren, S.D. Pike, I. Pernik, A.S. Weller, M.C. Willis, Organometallics 34 (2015) 711–723.
[31] J.F. Hooper, A.B. Chaplin, C. González-Rodríguez, A.L. Thompson, A.S. Weller, M. C. Willis, J. Am. Chem. Soc. 134 (2012) 2906–2909.
[32] S. Hillebrand, J. Bruckmann, C. Krüger, M.W. Haenel, Tetrahedron Lett. 36 (1995) 75–78.
[33] G.L. Williams, C.M. Parks, C.R. Smith, H. Adams, A. Haynes, A.J.H.M. Meijer, G.J. Sunley, S. Gaemers, Organometallics 30 (2011) 6166–6179.
[34] A.J. Sandee, L.A. van der Veen, J.N.H. Reek, P.C.J. Kamer, M. Lutz, A.L. Spek, P.W. N.M. van Leeuwen, Angew. Chem. Int. Ed. 38 (1999) 3231–3235.
[35] G.J. Kubas, J. Organomet. Chem. 751 (2014) 33–49.
[36] R.J. van Haaren, K. Goubitz, J. Fraanje, G.P.F. van Strijdonck, H. Oevering, B. Coussens, J.N.H. Reek, P.C.J. Kamer, P.W.N.M. van Leeuwen, Inorg. Chem. 40 (2001) 3363–3372.
[37] A.M. Johns, M. Utsunomiya, C.D. Incarvito, J.F. Hartwig, J. Am. Chem. Soc. 128 (2006) 1828–1839.
[38] B.Z. Momeni, R. Kia, S. Ghanbarzadeh, Monatsch. Chem. 143 (2012) 1479–1486.
[39] A.J. Pontiggia, A.B. Chaplin, A.S. Weller, J. Organomet. Chem. 696 (2011) 2870–2876.
[40] J.-A. Dimmer, M. Hornung, T. Wütz, L. Wesemann, Organometallics 31 (2012) 7044–7051.
[41] M.A. Zuideveld, B.H.G. Swennenhuis, M.D.K. Boele, Y. Guari, G.P.F. van Strijdonck, J.N.H. Reek, P.C.J. Kamer, K. Goubitz, J. Fraanje, M. Lutz, A.L. Spek, P.W.N.M. van Leeuwen, J. Chem. Soc., Dalton Trans. (2002) 2308–2317.
[42] K.Q. Almeida Lenero, Y. Guari, P.C.J. Kamer, P.W.N.M. van Leeuwen, B. Donnadieu, S. Sabo-Etienne, B. Chaudret, M. Lutz, A.L. Spek, Dalton Trans. 42 (2013) 6495–6512.
[43] E.A. Standley, S.J. Smith, P. Müller, T.F. Jamison, Organometallics 33 (2014) 2012–2018.
[44] J. Yin, S.L. Buchwald, J. Am. Chem. Soc. 124 (2002) 6043–6048.
[45] R.A. Stockland, A.M. Levine, M.T. Giovine, I.A. Guzei, J.C. Cannistra, Organometallics 23 (2004) 647–656.
[46] V.V. Grushin, W.J. Marshall, J. Am. Chem. Soc. 128 (2006) 12644–12645.
[47] V.I. Bakhmutov, F. Bozoglian, K. Gómez, G. González, V.V. Grushin, S.A. Macgregor, E. Martin, F.M. Miloserdov, M.A. Novikov, J.A. Panetier, L.V. Romashov, Organometallics 31 (2012) 1315–1328.
[48] Y. Guari, G.P.F. van Strijdonck, M.D.K. Boele, J.N.H. Reek, P.C.J. Kamer, P.W.N.M. van Leeuwen, Chem. Eur. J. 7 (2001) 475–482.
[49] D.J. Fox, S.B. Duckett, C. Flaschenriem, W.W. Brennessel, J. Schneider, A. Gunay, R. Eisenberg, Inorg. Chem. 45 (2006) 7197–7209.
[50] F.M. Miloserdov, C.L. McMullin, M. Martınez Belmonte, J. Benet-Buchholz, V.I. Bakhmutov, S.A. Macgregor, V.V. Grushin, Organometallics 33 (2014) 736–752.
[51] Y.-Y. Jiang, H.-Z. Yu, Y. Fu, Organometallics 32 (2013) 926–936.
[52] H. Kinuta, H. Takahashi, M. Tobisu, S. Mori, N. Chatani, Bull. Chem. Soc. Jpn. 87 (2014) 655–669.
[53] A.A. Ruch, S. Handa, F. Kong, V.N. Nesterov, D.R. Pahls, T.R. Cundari, L.M. Slaughter, Org. Biomol. Chem. 14 (2016) 8123–8140.
[54] A. Wu, B.O. Patrick, E. Chung, B.R. James, Dalton Trans. 41 (2012) 11093–11106.
[55] A.E.W. Ledger, P.A. Slatford, J.P. Lowe, M.F. Mahon, M.K. Whittlesey, J.M.J. Williams, Dalton Trans. (2009) 716–722.
[56] H.C. Johnson, E.M. Leitao, G.R. Whittell, I. Manners, G.C. Lloyd-Jones, A.S. Weller, J. Am. Chem. Soc. 136 (2014) 9078–9093.
[57] D. Fujino, H. Yorimitsu, A. Osuka, J. Am. Chem. Soc. 136 (2014) 6255–6258.
[58] J. Alós, T. Bolaño, M.A. Esteruelas, M. Oliván, E. Oñate, M. Valencia, Inorg. Chem. 52 (2013) 6199–6213.
[59] M.A. Esteruelas, C. García-Yebra, J. Martín, E. Oñate, Inorg. Chem. 56 (2017) 676–683.
[60] M.A. Esteruelas, I. Fernández, C. García-Yebra, J. Martín, E. Oñate, Organometallics 36 (2017) 2298–2307.
[61] M.C. Haibach, D.Y. Wang, T.J. Emge, K. Krogh-Jespersen, A.S. Goldman, Chem. Sci. 4 (2013) 3683–3692.
[62] J.-Y. Hu, J. Zhang, G.-X. Wang, H.-L. Sun, J.-L. Zhang, Inorg. Chem. 55 (2016) 2274–2283.
[63] D.V. Partyka, J.B. Updegraff III, M. Zeller, A.D. Hunter, T.G. Gray, Dalton Trans. 39 (2010) 5388–5397.
[64] A. Pintado-Alba, H. de la Riva, M. Nieuwhuyzen, D. Bautista, P.R. Raithby, H.A. Sparkes, S.J. Teat, J.M. Lopez-de-Luzuriaga, M.C. Lagunas, Dalton Trans. (2004) 3459–3467.
[65] M.A. Esteruelas, P. Nolis, M. Oliván, E. Oñate, A. Vallribera, A. Vélez, Inorg. Chem. 55 (2016) 7176–7181.
[66] Z.Y. Xu, Y.Y. Jiang, W. Su, H.Z. Yu, Y. Fu, Chem. Eur. J. 22 (2016) 14611–14617.
[67] M.W. Haenel, D. Jakubik, E. Rothenberger, G. Schroth, Chem. Ber. 124 (1991) 1705–1710.
[68] E.M. Vogl, J. Bruckmann, C. Krüger, M.W. Haenel, J. Organomet. Chem. 520 (1996) 249–252.
[69] S.-M. Kuang, P.E. Fanwick, R.A. Walton, Inorg. Chem. 41 (2002) 405–412.
[70] E.M. Vogl, J. Bruckmann, M. Kessler, C. Krüger, M.W. Haenel, Chem. Ber. 130 (1997) 1315–1319.
[71] R. Venkateswaran, M.S. Balakrishna, S.M. Mobin, H.M. Tuononen, Inorg. Chem. 46 (2007) 6535–6541.
[72] R. Venkateswaran, J.T. Mague, M.S. Balakrishna, Inorg. Chem. 46 (2007) 809–817.
[73] R. Dallanegra, A.B. Chaplin, A.S. Weller, Organometallics 31 (2012) 2720–2728.
[74] P.W.N.M. van Leeuwen, M.A. Zuideveld, B.H.G. Swennenhuis, Z. Freixa, P.C.J. Kamer, K. Goubitz, J. Fraanje, M. Lutz, A.L. Spek, J. Am. Chem. Soc. 125 (2003) 5523–5539.
[75] R.J. Pawley, M.A. Huertos, G.C. Lloyd-Jones, A.S. Weller, M.C. Willis, Organometallics 31 (2012) 5650–5659.
[76] T. Ohshima, Y. Miyamoto, J. Ipposhi, Y. Nakahara, M. Utsunomiya, K. Mashima, J. Am. Chem. Soc. 131 (2009) 14317–14328.
[77] T.E. Stevens, K.A. Smoll, K.I. Goldberg, J. Am. Chem. Soc. 139 (2017) 7725–7728.
[78] M. Utsunomiya, R. Kuwano, M. Kawatsura, J.F. Hartwig, J. Am. Chem. Soc. 125 (2003) 5608–5609.
[79] A. Couce-Rios, A. Lledós, G. Ujaque, Chem. Eur. J. 22 (2016) 9311–9320.
[80] W. Goertz, P.C.J. Kamer, P.W.N.M. van Leeuwen, D. Vogt, Chem. Eur. J. 7 (2001) 1614–1618.
[81] L.D. Julian, J.F. Hartwig, J. Am. Chem. Soc. 132 (2010) 13813–13822.
[82] M.W. Haenel, H. Fieseler, D. Jakubik, B. Gabor, R. Goddard, C. Krüger, Tetrahedron Lett. 34 (1993) 2107–2110.
[83] K. Aurivillius, L. Fälth, Chem. Scr. 4 (1973) 215–218.
[84] L. Fälth, Chem. Scr. 9 (1976) 167–170.
[85] L.V. Andreasen, O. Simonsen, O. Wernberg, Inorg. Chim. Acta 295 (1999) 153–163.
[86] L.V. Andreasen, A. Hazell, O. Wernberg, Acta Crystallogr., Sect. C 58 (2002) m385–m387.
[87] F. Tisato, F. Refosco, M. Porchia, C. Bolzati, G. Bandoli, A. Dolmella, A. Duatti, A. Boschi, C.M. Jung, H.-J. Pietzsch, W. Kraus, Inorg. Chem. 43 (2004) 8617–8625.
[88] D.J.H. Emslie, L.E. Harrington, H.A. Jenkins, C.M. Robertson, J.F. Britten, Organometallics 27 (2008) 5317–5325.
[89] M. Naoya, A. Yuki, T. Shinya, N. Kensuke, K. Takashi, H. Tetsutaro, Chem. Lett. 37 (2008) 418–419.
[90] I.J. Bruno, J.C. Cole, P.R. Edgington, M. Kessler, C.F. Macrae, P. McCabe, J. Pearson, R. Taylor, Acta Crystallogr., Sect. B 58 (2002) 389–397.
[91] C.R. Groom, I.J. Bruno, M.P. Lightfoot, S.C. Ward, Acta Crystallogr., Sect. B 72 (2016) 171–179.
[92] The CSD search was conducted using the ConQuest package (CSD version 5.38, update 3, May 2017). See supporting materials for the output of this search including CSD reference codes.